Spectroscopy®
Solutions for Materials Analysis

CEM

LC, GC, or ICP — We have the sample prep solution for you.

A New Revolution in Solvent Extraction

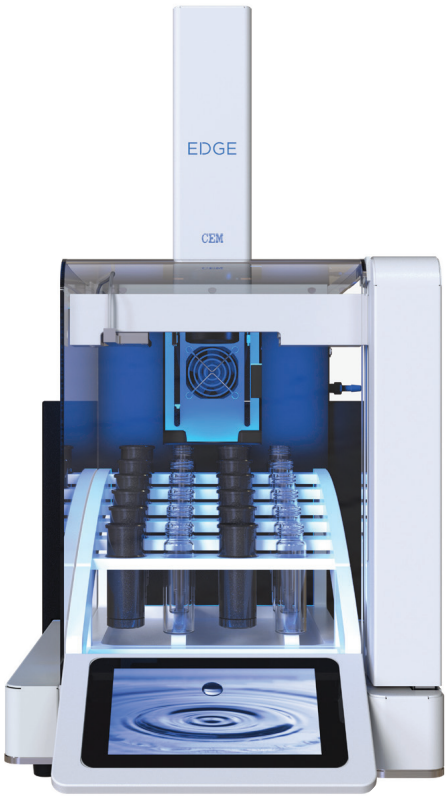

Better Digestions Better Analyses

We Simplify Science

cem.com

Learn more about how CEM can simplify your sample prep at cem.com

EDGE™

Energized Dispersive Guided Extraction

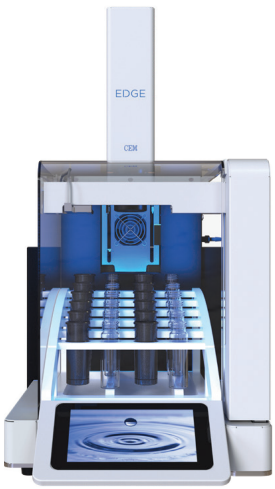

Benefits

- 5-minute extractions
- Simple assembly
- Exceptional recoveries

Extract

- SVOCs in soil (EPA 3545A)
- Pesticides in food
- Phthalates in plastics

cem.com/EDGE

MARS™6

Microwave Digestion System

Benefits

- Industry leading technology support
- Simple to assemble vessels
- Better digestions for better analyses

Digest

- Large samples
- Tough samples
- Almost any sample

cem.com/MARS6

Learn more about how CEM can simplify your sample prep at cem.com

Spectroscopy®

Solutions for Materials Analysis

September 2018 Volume 33 Number 9 www.spectroscopyonline.com

Micro-Raman Microspectroscopy Analysis of Graphite Mechanical Behavior

New Frontiers in Infrared Spectroscopy

Infrared Microspectroscopy Mapping at Submicrometer Spatial Resolution

A Flexible Analytical Data Life Cycle?

UBM

RAPID, ACCURATE MID-INFRARED ANALYSIS

The **Ocean MZ5** is a fast, scalable alternative to traditional FTIR spectroscopy for **chemical identification**, **food authentication** and **environmental testing**. This self-contained system requires no accessories and measures absorbance and transmittance of liquid samples **from 1818–909 cm-1 (5.5-11 µm)**.

Ocean Optics

www.oceanoptics.com

info@oceanoptics.com • US +1 727-733-2447 • EUROPE +31 26-3190500 • ASIA +86 21-6295-6600

State-of-the-Art X-Ray Solutions

•FAST SDD® •SDD •Si-PIN

In-house manufacturing = The highest performing detectors available

The best detector for optimal results

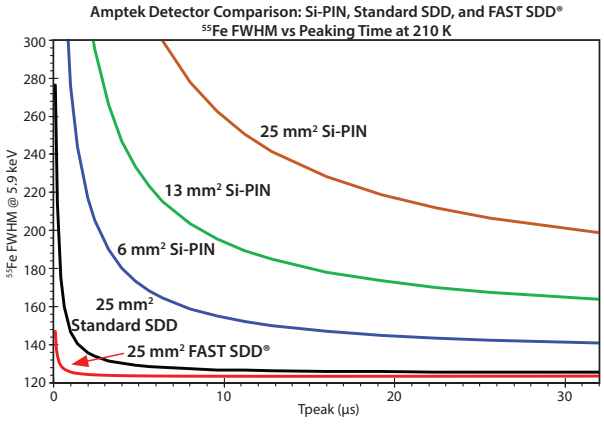

FAST SDD® Detector

>2,000,000 CPS and 122 eV FWHM Resolution

Options:

- 25 mm² collimated to 17 mm²
- 70 mm² collimated to 50 mm²
- Windows: Be (0.5 mil) 12.5 µm, or C Series (Si_3N_4)
- TO-8 package fits all Amptek configurations

Configurations to meet your needs

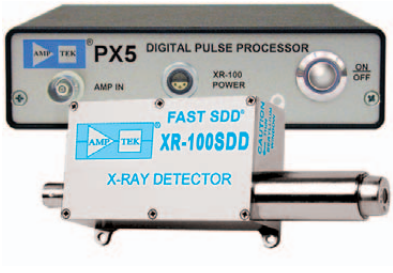

XR-100 and PX5 Digital Pulse Processor

X-123 Complete X-Ray Spectrometer

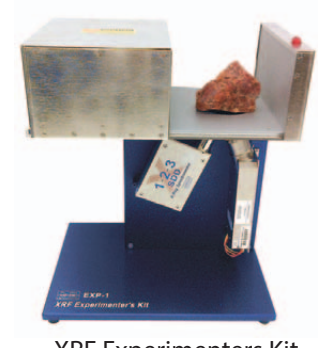

XRF Experimenters Kit

OEM Configurations

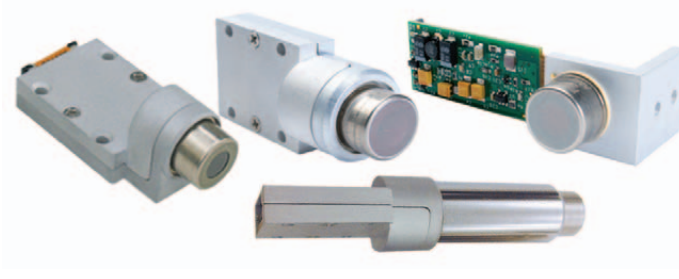

A sample of detectors with preamplifiers and heat sinks

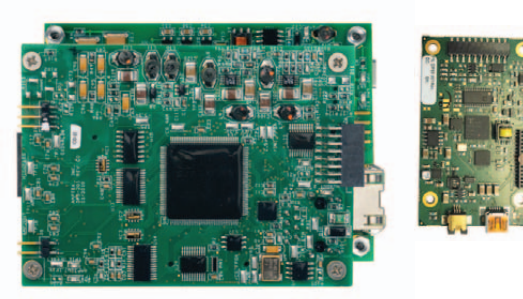

Digital Pulse Processors and Power Supplies

AMP TEK®

OEM's #1 Choice For XRF

amptek.com

AMETEK® MATERIALS ANALYSIS DIVISION

LP980
Transient Absorption Spectrometer

EDINBURGH INSTRUMENTS

FLS1000
Photoluminescence Spectrometer

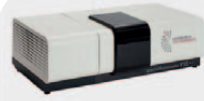

FS5
Spectrofluorometer

EXPERTS IN FLUORESCENCE SPECTROSCOPY

Key Techniques:

> Time-Resolved Fluorescence
> Steady State Fluorescence
> Phosphorescence Lifetime
> Transient Absorption

edinst.com

1000+
high-specification systems in industry and leading universities

EOT
Electro-Optics Technology, Inc.
Tornos Series
Compact Optical Isolators
Effectively *eliminate* optical feedback.

- Compact design suitable for OEM integration
- Tunable over a wide spectral range
- Optional waveplate for polarization manipulation

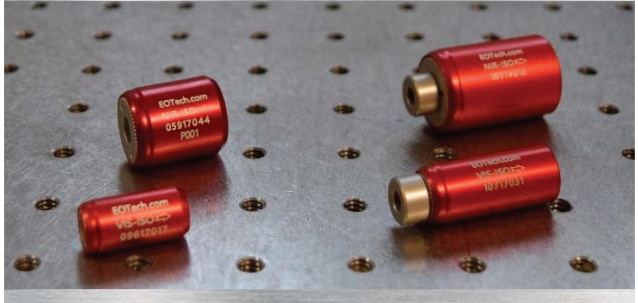

High Quality | Great Performance
EOT www.eotech.com | sales@eotech.com
Electro-Optics Technology, Inc. 231-935-4044

Spectroscopy®

MANUSCRIPTS: To discuss possible article topics or obtain manuscript preparation guidelines, contact the editorial director at: (732) 346-3020, e-mail: Laura.Bush@ubm.com. Publishers assume no responsibility for safety of artwork, photographs, or manuscripts. Every caution is taken to ensure accuracy, but publishers cannot accept responsibility for the information supplied herein or for any opinion expressed.

SUBSCRIPTIONS: For subscription information: *Spectroscopy,* P.O. Box 6196, Duluth, MN 55806-6196; (888) 527-7008, 7:00 a.m. to 6:00 p.m. CST. Outside the U.S., +1-218-740-6477. Delivery of *Spectroscopy* outside the U.S. is 3–14 days after printing. Single-copy price: U.S., $10.00 + $7.00 postage and handling ($17.00 total); Canada and Mexico, $12.00 + $7.00 postage and handling ($19.00 total); Other international, $15.00 + $7.00 postage and handling ($22.00 total).

CHANGE OF ADDRESS: Send change of address to *Spectroscopy,* P.O. Box 6196, Duluth, MN 55806-6196; provide old mailing label as well as new address; include ZIP or postal code. Allow 4–6 weeks for change. Alternately, go to the following URL for address changes or subscription renewal: http://ubmsubs.ubm.com/?pubid=SPEC

RETURN ALL UNDELIVERABLE CANADIAN ADDRESSES TO: IMEX Global Solutions, P.O. Box 25542, London, ON N6C 6B2, CANADA. PUBLICATIONS MAIL AGREEMENT No.40612608.

REPRINT SERVICES: Reprints of all articles in this issue and past issues are available (500 minimum). Licensing and Reuse of Content: Contact our official partner, Wright's Media, about available usages, license fees, and award seal artwork at Advanstar@wrightsmedia.com for more information. Please note that Wright's Media is the only authorized company that we've partnered with for Advanstar UBM materials.

C.A.S.T. DATA AND LIST INFORMATION: Contact Melissa Stillwell, (218) 740-6831; e-mail: Melissa.Stillwell@ubm.com

INTERNATIONAL LICENSING: Jillyn Frommer, (732) 346-3007, fax: (732) 647-1104; e-mail:Jillyn.Frommer@ubm.com

50% Recycled Paper 10-20% Post Consumer Waste

Alliance for Audited Media

© 2018 UBM. All rights reserved. No part of this publication may be reproduced or transmitted in any form or by any means, electronic or mechanical including by photocopy, recording, or information storage and retrieval without permission in writing from the publisher. Authorization to photocopy items for internal/educational or personal use, or the internal/educational or personal use of specific clients is granted by UBM for libraries and other users registered with the Copyright Clearance Center, 222 Rosewood Dr. Danvers, MA 01923, 978-750-8400 fax 978-646-8700 or visit http://www.copyright.com online. For uses beyond those listed above, please direct your written request to Permission Dept. fax 732-647-1104 or email: Jillyn.Frommer@ubm.com.

UBM Americas provides certain customer contact data (such as customers' names, addresses, phone numbers, and e-mail addresses) to third parties who wish to promote relevant products, services, and other opportunities that may be of interest to you. If you do not want UBM Americas to make your contact information available to third parties for marketing purposes, simply call toll-free 866-529-2922 between the hours of 7:30 a.m. and 5 p.m. CST and a customer service representative will assist you in removing your name from UBM Americas lists. Outside the U.S., please phone 218-740-6477.

Spectroscopy does not verify any claims or other information appearing in any of the advertisements contained in the publication, and cannot take responsibility for any losses or other damages incurred by readers in reliance of such content.

Spectroscopy welcomes unsolicited articles, manuscripts, photographs, illustrations and other materials but cannot be held responsible for their safekeeping or return.

To subscribe, call toll-free 888-527-7008. Outside the U.S. call 218-740-6477.

UBM Americas (www.ubmamericas.com) is a leading worldwide media company providing integrated marketing solutions for the Fashion, Life Sciences and Powersports industries. UBM Americas serves business professionals and consumers in these industries with its portfolio of 91 events, 67 publications and directories, 150 electronic publications and Web sites, as well as educational and direct marketing products and services. Market leading brands and a commitment to delivering innovative, quality products and services enables UBM Americas to "Connect Our Customers With Theirs. UBM Americas has approximately 1000 employees and currently operates from multiple offices in North America and Europe.

Flexible, Aberration-Free Raman Spectroscopy ...Now for Inorganic Materials

FERGIE Raman microscopy setup with 532 nm Raman CUBE

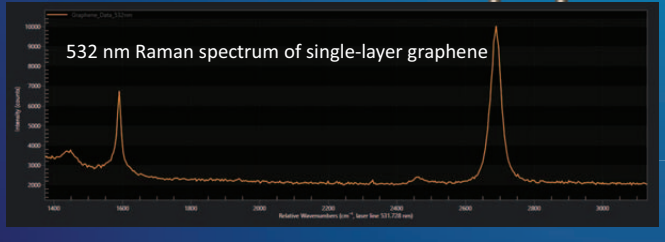

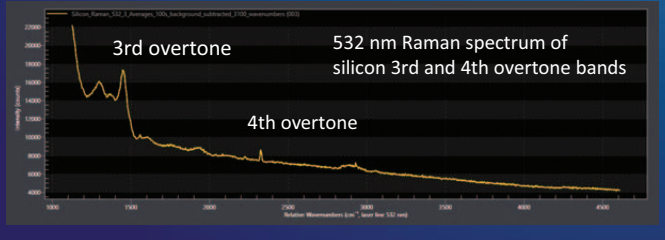

FERGIE's ecosystem has expanded!

FERGIE® makes it easier than ever to conduct even challenging Raman measurements on inorganic and semiconductor materials with a new set of 532 nm accessories, including:

- F-matched focusing CUBES
- Raman CUBES with fully aligned Raman notch and clean-up filters

Hear what researchers are saying about FERGIE at www.fergiespec.com

Princeton Instruments

Global Sales & Support
www.princetoninstruments.com
info@princetoninstruments.com
tel: +1 609.587.9797

Certified Reference Materials for Instrument Qualification

The widest range:
Deep UV to Infra-red
Up to 3.5 Absorbance
NIST Traceable
ISO 17034 Reference Material Producer
ISO/IEC 17025 accredited supplier
Lifetime Guarantee
Fast Recalibration Service
Meet all International regulatory Standards

Starna
Starna Cells, Inc.
PO Box 1919 Atascadero, CA 93423
Phone: (800) 228-4482 USA or (805) 466-8855 outside USA
sales@starnacells.com www.starnacells.com

2018 EASTERN ANALYTICAL SYMPOSIUM & EXPOSITION
ANALYTICAL SOLUTIONS
TO THE WORLD'S PROBLEMS
November 12-14, 2018
Crowne Plaza Princeton Conference Center
Plainsboro, NJ

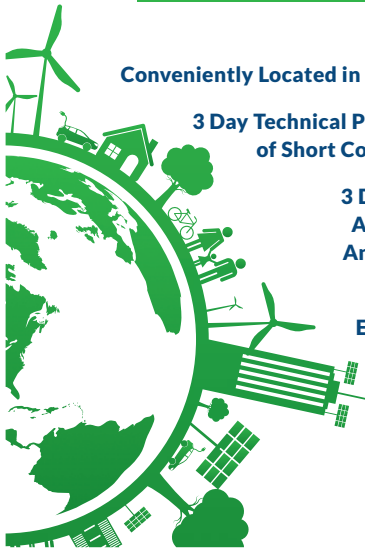

Conveniently Located in Central New Jersey
3 Day Technical Program with 4 Days of Short Courses and Seminars
3 Day Exposition with Access to Vendors of Analytical Equipment
Workshops and Employment Bureau

eas.org

Spectroscopy®

485F US Highway One South, Suite 210
Iselin, NJ 08830
(732) 596-0276
Fax: (732) 647-1235

Michael J. Tessalone
Vice President/Group Publisher
Michael.Tessalone@ubm.com

Stephanie Shaffer
Publisher
Stephanie.Shaffer@ubm.com

Edward Fantuzzi
Associate Publisher
Edward.Fantuzzi@ubm.com

Michael Kushner
Senior Director, Digital Media
Michael.Kushner@ubm.com

Laura Bush
Editorial Director
Laura.Bush@ubm.com

John Chasse
Managing Editor
John.Chasse@ubm.com

Stephen A. Brown
Group Technical Editor
Stephen.Brown@ubm.com

Cindy Delonas
Associate Editor
Cindy.Delonas@ubm.com

Kristen Moore
Webcast Operations Manager
Kristen.Moore@ubm.com

Vania Oliveira
Project Manager
Vania.Oliveira@ubm.com

Sabina Advani
Digital Production Manager
Sabina.Advani@ubm.com

Kaylynn Chiarello-Ebner
Managing Editor, Special Projects
Kaylynn.Chiarello.Ebner@ubm.com

Dan Ward
Art Director
dward@hcl.com

Brianne Pangaro
Marketing Associate
Brianne.Pangaro@ubm.com

Melissa Stillwell
C.A.S.T. Data and List Information
Melissa.Stillwell@ubm.com

Thomas W. Ehardt
Executive Vice-President, Senior Managing Director
UBM Life Sciences Group
Tom.Ehardt@ubm.com

Dave Esola
VP & General Manager
UBM Life Sciences Group
Dave.Esola@ubm.com

Jillyn Frommer
Permissions
Jillyn.Frommer@ubm.com

Jesse Singer
Production Manager
jsinger@hcl.com

Wendy Bong
Audience Development Manager
Wendy.Bong@ubm.com

Ross Burns
Audience Development Assistant Manager
Ross.Burns@ubm.com

Portable Hydraulic Press

Make high-quality KBr pellets with the turn of a knob using the PIKE Pixie portable hydraulic press. Simply load your powdered KBr/sample matrix into the die chamber then set the assembled die onto the platform of the press. Force up to 2.5 tons may be applied. Place the die collar containing the newly formed pellet into a holder and position it in the spectrometer's 2 x 3" slide mount holder for measurement. Pixie's small footprint makes it easy to store and is ideal for limited bench space environments and glove boxes.

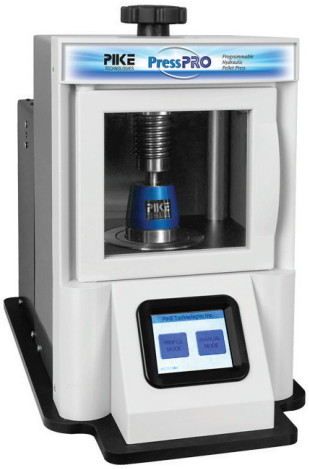

IR Pellet Perfection

PIKE Technologies introduces PressPRO, a microprocessor controlled automated hydraulic press designed to produce consistently superior KBr pellets and enhance the uniformity and quality of transmission samples. PressPRO is capable of a variable force from 1 to 15 US tons. Up to four pressure hold time and ramps may be programmed and performed within a run, and five profiles may be stored on the device.

PRESSING MATTERS

At PIKE Technologies, we understand the art of KBr pellet making and its importance to FTIR sampling. High-quality pellets equate to spectral reproducibility and success with difficult or limited-mass samples.

We offer a full line of transmission sampling tools and accessories that produce superior spectra and make sampling easier, including:

- **Hydraulic Presses**
- **Evacuable Pellet Press**
- **Manual, Economy Presses**
- **Heavy-Duty Sample Grinders**
- **Mortars and Pestles**
- **KBr Chunks and Powder and More!**

FIND ALL THE SAMPLE PREPARATION TOOLS YOU NEED AT www.piketech.com

PIKE TECHNOLOGIES

info@piketech.com
(608) 274-2721

Spectroscopy
September 2018
Volume 33 Number 9

Cover image courtesy of koya979/Shutterstock.

ON THE WEB

QUIZ: INTERPRETING SPECTRA

Take the latest quiz!

Are your spectral interpretation skills up to par? Find out by taking the latest quiz from our "IR Spectral Interpretation Workshop" column.

See the quiz on page 26 of this issue or at:

www.spectroscopyonline.com/ir-spectral-interpretation-workshop-0

WEB SEMINARS

Discover How Triple Quadrupole ICP-MS Will Help You Do More and Simplify Your Laboratory Routines

Daniel Kutscher and Simon Nelms, Thermo Fisher Scientific

Any Sample, Any Time: The Benefits of Single Reaction Chamber Microwave Digestion for Trace Element Analysis

Robert Thomas, Scientific Solutions
Laura Thompson, Milestone Inc.

spectroscopyonline.com/spec/webcasts

Like *Spectroscopy* on Facebook:
www.facebook.com/SpectroscopyMagazine

Follow *Spectroscopy* on Twitter:
https://twitter.com/spectroscopyMag

Join the *Spectroscopy* Group on LinkedIn
http://linkd.in/SpecGroup

CONTENTS

VOLUME 33 NUMBER 9
SEPTEMBER 2018

COLUMNS

Molecular Spectroscopy Workbench 12
Advances in Infrared Microspectroscopy and Mapping Molecular Chemical Composition at Submicrometer Spatial Resolution
John A. Reffner
Infrared microspectroscopy has led to important advances in a wide range of fields, as biologists, chemists, geologists, materials scientists, microscopists, and spectroscopists around the world have awakened to the value of nanotechnology. The small world is getting larger.

Focus on Quality 18
A Flexible Analytical Data Life Cycle?
R.D. McDowall
Does a one-size-fits-all data life cycle meet laboratory requirements for data integrity? No! The reason is that there are many different types of analytical procedures, which means that a flexible analytical data life cycle is needed.

IR Spectral Interpretation Workshop 24
The C=O Bond, Part VII: Aromatic Esters, Organic Carbonates, and More of the Rule of Three
Brian C. Smith
Aromatic esters follow the ester Rule of Three, but each of these three peak positions is different for saturated and aromatic esters, which makes them easy to distinguish. Organic carbonates are structurally similar to esters and follow their own Rule of Three.

ARTICLES

Identification of Graphite Mechanical Behavior and Dislocations by Micro-Raman Microscopy 30
Ram Krishna and Paul M. Mummery
In this study, micro-Raman microscopy was used to examine graphite mechanical behavior through the evolution of dislocation defect density and the resultant deformation (strain) in graphite components. The increasing strength of the Raman optical phonon modes linked with a generous number of dislocations indicates the potential capability of Raman spectroscopy to help develop a mechanistic understanding of the complex mechanical behavior of graphite for use in many industries and applications.

Infrared Spectroscopy: New Frontiers Both Near and Far 34
Negar Atefi, Tanvi Vakil, Zahra Abyat, Sarvesh K. Ramlochun, Gorkem Bakir, Ian M.C. Dixon, Benedict C. Albensi, Tanya E.S. Dahms, and Kathleen M. Gough
This article illustrates experience with some new developments in IR spectroscopy, with examples of how this traditional field continues to explode into new territory, enabling rapid acquisition of huge data sets on the one hand, while permitting exploration of chemical composition of targets with nanometer-scale spatial resolution on the other.

THE APPLICATION NOTEBOOK 43

DEPARTMENTS

Products & Resources 39
Ad Index 42

Spectroscopy (ISSN 0887-6703 [print], ISSN 1939-1900 [digital]) is published monthly by UBM LLC 131 West First Street, Duluth, MN 55802-2065. Spectroscopy is distributed free of charge to users and specifiers of spectroscopic equipment in the United States. *Spectroscopy* is available on a paid subscription basis to nonqualified readers at the rate of: U.S. and possessions: 1 year (12 issues), $74.95; 2 years (24 issues), $134.50. Canada/Mexico: 1 year, $95; 2 years, $150. International: 1 year (12 issues), $140; 2 years (24 issues), $250. Periodicals postage paid at Duluth, MN 55806 and at additional mailing offices. POSTMASTER: Send address changes to Spectroscopy, P.O. Box 6196, Duluth, MN 55806-6196. PUBLICATIONS MAIL AGREEMENT NO. 40612608, Return Undeliverable Canadian Addresses to: IMEX Global Solutions, P. O. Box 25542, London, ON N6C 6B2, CANADA. Canadian GST number: R-124213133RT001. Printed in the U.S.A.

Expectations surpassed. Quality assured.

- Unrivaled technology
- Safety by design
- Maximum throughput
- Lower operating costs

Milestone sets the standard for microwave digestion excellence.

You make important choices for your lab every day – decisions that can impact the quality of your analyses, the efficiency of your processes and the reliability of your operation. With three decades of technology firsts, including over thirty patents, Milestone instruments offer the most innovative metals prep technology on the market today.

With a complete digestion product line that includes the revolutionary UltraWAVE and powerful Ethos UP, Milestone is the first choice of laboratories that rely on quality sample prep for superior ICP/ICP-MS analyses.

See what Milestone can do for your lab.
Learn more about Milestone digestion products at www.milestonesci.com or call us at 866.995.5100.

milestone connect

Ethos UP

UltraWAVE

UltraCLAVE

Download our **FREE PRIMER: USP 232/233 and 2232 Compliance -** Getting ready for heavy metals testing.

https://milestonesci.com/usp-primer-download

MILESTONE

Editorial Advisory Board

Fran Adar Horiba Scientific

Russ Algar University of British Columbia

Matthew J. Baker University of Strathclyde

Ramon M. Barnes University of Massachusetts

Matthieu Baudelet University of Central Florida

Rohit Bhargava University of Illinois at Urbana-Champaign

Paul N. Bourassa Blue Moon Inc.

Michael S. Bradley Thermo Fisher Scientific

Deborah Bradshaw Consultant

Lora L. Brehm The Dow Chemical Company

George Chan Lawrence Berkeley National Laboratory

John Cottle University of California Santa Barbara

David Lankin University of Illinois at Chicago, College of Pharmacy

Barbara S. Larsen DuPont Central Research and Development

Bernhard Lendl Vienna University of Technology (TU Wien)

Ian R. Lewis Kaiser Optical Systems

Rachael R. Ogorzalek Loo University of California Los Angeles, David Geffen School of Medicine

Howard Mark Mark Electronics

R.D. McDowall McDowall Consulting

Gary McGeorge Bristol-Myers Squibb

Linda Baine McGown Rensselaer Polytechnic Institute

Francis M. Mirabella Jr. Mirabella Practical Consulting Solutions, Inc.

Ellen V. Miseo Illuminate

Michael L. Myrick University of South Carolina

John W. Olesik The Ohio State University

Steven Ray State University of New York at Buffalo

Jim Rydzak Specere Consulting

Jerome Workman Jr. Unity Scientific

Lu Yang National Research Council Canada

Spectroscopy's Editorial Advisory Board is a group of distinguished individuals assembled to help the publication fulfill its editorial mission to promote the effective use of spectroscopic technology as a practical research and measurement tool. With recognized expertise in a wide range of technique and application areas, board members perform a range of functions, such as reviewing manuscripts, suggesting authors and topics for coverage, and providing the editor with general direction and feedback. We are indebted to these scientists for their contributions to the publication and to the spectroscopy community as a whole.

RENISHAW
apply innovation™

Next generation Raman imaging

High performance Raman systems for a range of applications

Raman spectroscopy produces chemical and structural images to help you understand more about the material being analysed. Renishaw has decades of experience developing flexible Raman systems that give reliable results, for even the most challenging measurements. With Renishaw's suite of Raman systems, you can see the small things, the large things and things you didn't even know were there.

Visit www.renishaw.com/raman

See us at booth #301 SCIX October 21 - 26, 2018

Renishaw Inc. 1001 Wesemann Drive, West Dundee, Illinois, 60118, United States
T +1 847 286 9953 F +1 847 286 9974 E raman@renishaw.com

www.renishaw.com

Inorganic Ventures gives you a little more control.

The key to accurate testing is control. It's also the key to managing your testing program. Inorganic Ventures offers more options in Certified Reference Materials (CRMs) to help you get the right tools to control testing accuracy and your budget.

Inorganic Ventures offers 30mL volumes on our 1,000 ppm and 10,000 ppm stock products, as well as our entire line of custom products.*

Benefits:

- No hazardous shipping fees
- Less waste
- Storage and contamination concerns minimized
- Packaged with TCT

**Some exclusions may apply.*

INORGANIC™ VENTURES

inorganicventures.com | 1.800.669.6799

300 Technology Drive | Christiansburg, VA 24073 USA

Molecular Spectroscopy Workbench

Advances in Infrared Microspectroscopy and Mapping Molecular Chemical Composition at Submicrometer Spatial Resolution

Although 69 years have passed since infrared spectroscopy and microscopy were first united, these technologies continue to advance. Since 1983, the catalysts for rapid commercial growth and broad applications were Fourier transform infrared (FT-IR) spectrometers, resulting in advances in all reflecting microscope optics and high sensitivity detectors. Today, quantum cascade lasers and scanning microscopy are emerging technologies that are demonstrating the ability that drastically improves resolving power and quality of spectral data collected from submicrometer-sized samples. This installment of "Molecular Spectroscopy Workbench" is a brief history and reports on the status of infrared microspectroscopy and its future promise.

John A. Reffner

Art conservationists, biologists, chemists, environmentalists, forensic scientists, geologists and materials scientists need the combination of chemical composition and morphological structure to analyze complex matter, solve problems, or identify small particulates. Scanning electron microscopy (SEM) provides imaging of morphological structure, and can be combined with X-ray spectroscopy for elemental analysis. However, molecular composition may only be inferred from X-ray spectra by quantitative elemental analysis. Infrared microspectroscopy provides both molecular chemical information and imaging of morphological structure, but is limited for elemental analysis. The success of both of these techniques is dependent on their ability to provide high quality spectral data at the highest possible spatial resolution. Recent discoveries in infrared microspectroscopy are advancing this approach to new levels of spectral quality and resolving power.

First, a brief history of infrared microspectroscopy. In 1949, two publications (1,2) heralded the practicality of infrared spectroscopy. Perkin-Elmer Corp. introduced the first commercial infrared microspectrometer in 1953, the Model 85 (3). A single-beam, sodium chloride prism, dispersive infrared spectrometer was coupled to an all-reflective light microscope. A four-bladed variable aperture located in the primary image plane defined the area of the sample that produced the transmission spectrum. The detector was a bolometer and the intensity of transmitted infrared radiation at each wavelength

was plotted by a strip chart recorder. A string connected to the variable slit in the spectrometer was attached to a cardioid cam, increasing the slit width to maintain a level of incident intensity as the wavelength was increased. However, the spectral resolution varied across the spectrum. Obtaining a transmittance spectrum required recording an I_o and I_{sample} single beam spectra, tabulating the intensity of each at periodic wavelengths, calculating the I_{sample}/I_o ratio, and replotting the data. Although this system was a novel research tool, it was not a commercial success.

Infrared microspectroscopy was essentially dormant until 1978, when V. Coats introduced the Nanospec IR20 microspectrometer. By combining a microprocessor computer, a liquid nitrogen–cooled solid-state detector, a variable-wavelength interference filter monochromator, and an all-reflecting optical microscope, Coats resurrected interest in IR microspectroscopy. His revolutionary contribution was overshadowed when Fourier transform infra-

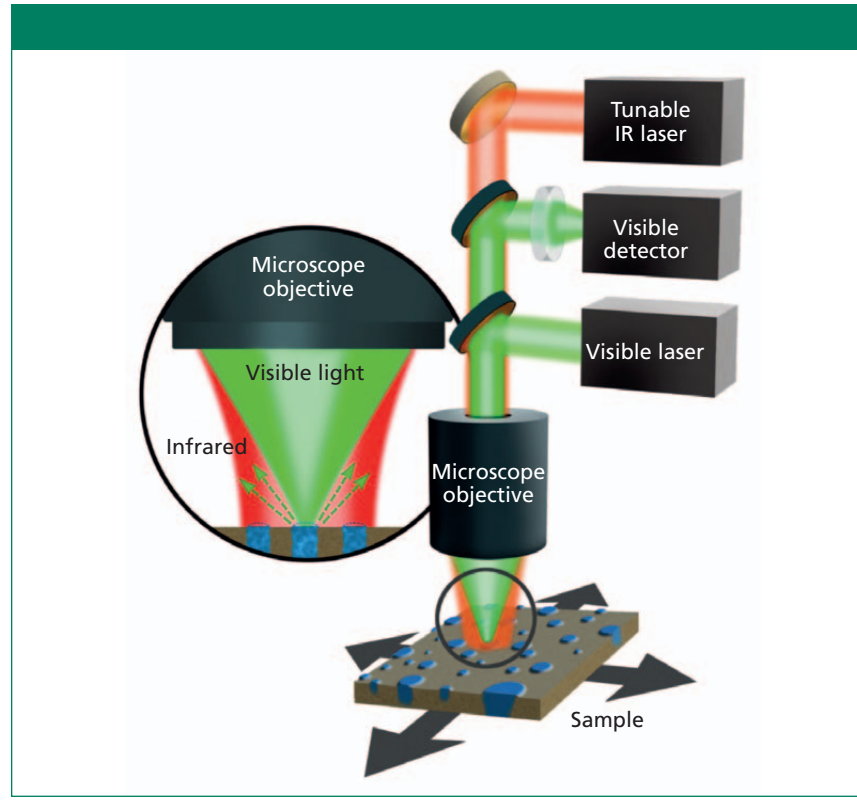

Figure 1: A schematic diagram illustrating the optical components of the mIRage photothermal infrared microspectrometer.

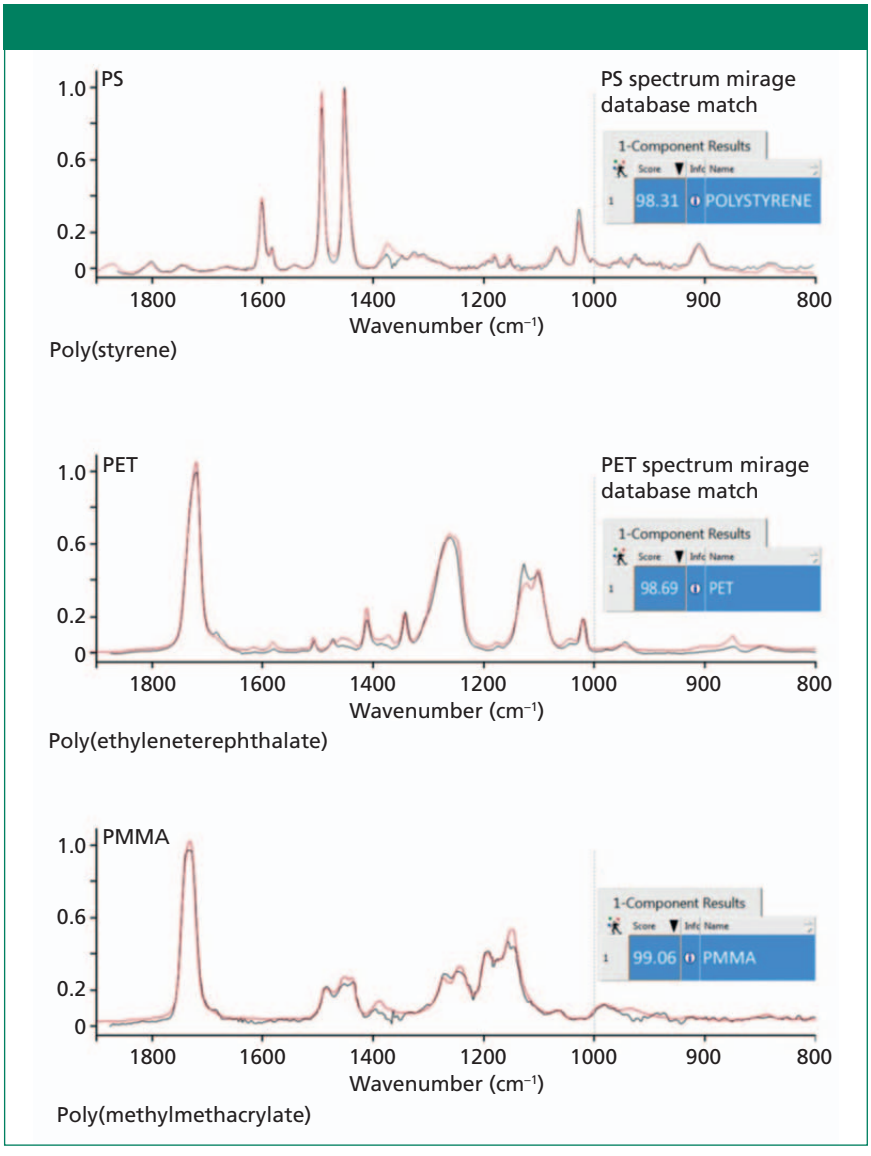

Figure 2: Infrared absorption spectra of poly(styrene) (PS), poly(ethyleneterephthalate) (PET), and poly(methylmethacrylate) (PMMA), collected using the mIRage photothermal infrared microspectrometer compared against the KnowItAll FT-IR spectral database (Bio-Rad) (in red).

red (FT-IR) spectrometers became commercially available. Attaching all reflecting microscopes to FT-IR spectrometers let the genie out of the bottle. Three decades of improvement to FT-IR microspectrometers, and sustained growth applications, established infrared microspectroscopy as a vital analytical technique.

The motto "good enough is never good enough" is a driving force for advancement. In microspectroscopy, improving spectral quality, detection limits, and resolving power are challenges. The quality of an infrared spectrum is limited by the intensity of incident radiation, wavelength resolution, sample size, and detector sensitivity. Detection limits are dependent on the sample's area, thickness, and composition. Resolving power—the minimal distance of separation of two objects—using visible or infrared radiation is limited by wavelength, numerical aperture, optics and contrast. The resolving power of spectral maps created using an FT-IR microspectrometer is limited by the wavelength and spectral contrast. The spectral quality and contrast of maps are reduced as the dimensions of the sample are reduced. When spectra are collected from a diffraction-limited point using an FT-IR spectrometer with a 1200 K ceramic source, spectral quality and contrast are reduced. Higher intensity sources, such as the synchrotron or quantum cascade (QC) lasers, have demonstrated improved spectral quality and mapping speed of performance at the wavelength diffraction limit.

United States Patent 457,709, filed April 4, 1994, lists the inventors F. Capasso, A.Y. Cho, J. Faist, A.I. Hutchinson, S. Luryi, C. Sirtori, and D.L. Sivco (4). The abstract of this patent states: "This application discloses, to the best of our knowledge, the first unipolar laser. An exemplary embodiment of the laser was implemented in the GaInAs/AlInAs system and emits radiation of about 4.2 μm wavelength. Embodiments in other material systems are possible, and the lasers can be readily designed to emit at a predetermined wavelength in a wide spectral region. We have designated the laser the 'Quantum Cascade' (QC) laser."

The foundation for the QC laser is the use of intersubband transitions for amplification of radiation (5). Over the past two decades, an abundance of QC laser research and development has been taking place (6). Today, QC lasers are commercially available from several sources. The power output has increased, and the operating temperature can be above room temperature. They can operate in either a continuous or pulsed mode. They are capable of emitting mid-infrared radiation in the 2857–400 cm^{-1} range. The successful application of QC lasers in medical, biological, environmental, communication, and chemical research has driven their expanding growth.

QC laser technology provides a new direction for advancing infrared microspectroscopy. The major avantages of QC lasers for infrared microspectroscopy are broad tunablity over the mid-infrared wavelength range, intensity, low divergence, and high frequency rate. Three approaches have been advanced for improving spatial resolution and quality of spectral data using QC lasers. The first approach was to replace the infrared radiation source with a broadly tunable QC laser for an all-reflecting microscope. The second approach was to couple the broadly tunable QC laser with scanning probe microscope to detect the photothermal expansion created by a modulated QC laser beam. The third approach was to

use a visible light probe to detect the photothermal expansion created by a modulated QC laser beam. These three approaches are addressed chronologically.

Replacing the thermal source with QC lasers was first demonstrated by the R. Bhargava research group at University of Illinois in Urbana, Illinois, in 2012. An in-house infrared microspectrometer was developed that used an array of tunable QC lasers supplied by DRS Daylight Solutions, tunable over the range of 1738 –1570 cm^{-1} as a transmitted radiation source (7). This microspectrometer system demonstrated that major advantage of using the QC laser over FT-IR was the speed of collection spectral maps using a single wavelength. In 2014, DSR Daylight Solutions introduced the first commercially available QC laser–powered chemical imaging microscope for IR spectroscopy. The Spero system (DSR Daylight Solutions) proclaimed real time, high-throughput spectral imaging enabled by ultrahigh-brightness QC laser technology. The spectral range of the Spero imaging system was expanded to 1800–900 cm^{-1}. This expanded range was a significant development. The initial applications these advances were in label-free histochemical imaging, and classification in tissues (8–11).

Combining QC laser technology with scanning probe microscopy (SPM) is the invention of C. Prater and K. Kjoller in 2011 (12–14). This invention makes possible a novel method for obtaining nanometer resolving power and high-resolution infrared spectra. The method includes using infrared radiation from a quantum cascade laser directed onto a small area of a sample. The QC laser array is tuned over a broad range of infrared wavelengths. When the sample adsorbs radiation of a certain wavelength, the energy of the adsorbed photon is transformed into heat, causing a thermal expansion of the sample. This photothermal event is monitored using a scanning probe microscope. The probe of the microscope is mounted on a cantilever. The QC laser is operated in a pulsed mode, creating a periodic motion of the cantilever. The amplitude of this osculation is a measure of the magnitude of the photothermal event. The magnitude of the thermal event plotted against the wavelength infrared radiation to produce a photothermal IR (PTIR) spectrum. This unique combination of QC laser and scanning probe technologies produces infrared spectra that are consistent with spectra collected by FT-IR. Photothermal IR is also known as atomic force infrared spectroscopy (AFM-IR).

AFM-IR advanced infrared spectroscopy from a resolving power limited by the wavelength of the infrared radiation to a limit defined by the tip size of the scanning probe, a change of scale from ~10 µm to ~10 nm. QC lasers provide the intensity to produce photothermal events that the scanning probe microscope detects to produce infrared spectra at subnanometer spatial resolution. The rapid scanning of the sample, while the it is exposed to a single wavelength of infrared radiation, produces molecular composition maps with unprecedented resolution.

B&WTEK
Your Mobile Spectroscopy Partner

All New QTRam™
Portable Raman System for Content and Blend Uniformity

Nondestructive quantitative transmission Raman analysis of solid dosage forms over a large sample volume.

No sample preparation, no solvents, with results in seconds.

Learn More About the QTRam
www.bwtek.com/NewQTRam

+1-302-368-7824 marketing@bwtek.com

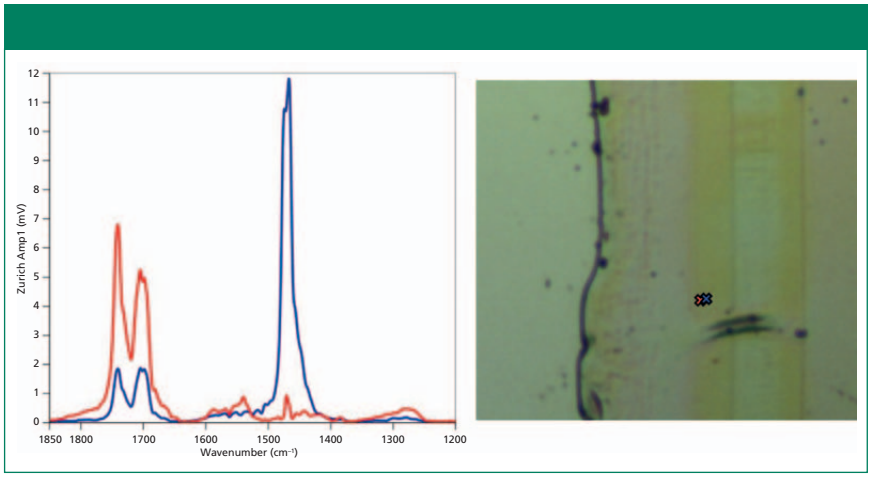

Figure 3: (Left) Photothermal infrared spectra collected using the mIRage system. (Right) Micrograph showing a digital image record of the cross-section of multilayered laminated sample. Two points, 500 nm apart, are marked with red and blue X's. The infrared spectra were collected at the indicated locations.

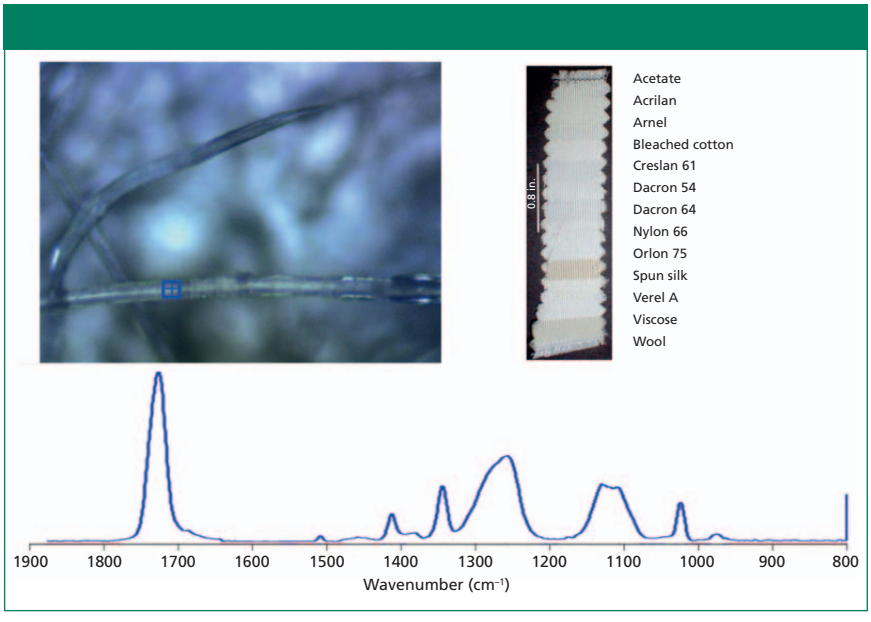

Figure 4: Optical image and O-PTIR spectrum of test fabric consisting of 13 different textile materials all woven together into a single sample. Data collected using the mIRage instrumentThe blue cross indicates the location where the O-PTIR spectrum was collected.

AFM-IR spectroscopy was the basis for the development by Anasys Instruments of the first commercial instrument, the nanoIR system (Anasys Instruments). The nanoIR instrument became available in 2012. In the past six years, AFM-IR technology has become a prominent tool in nano research in the biological, medical, chemical and materials sciences (14-16). The best evidence for the success of AFM–IR is the recent acquisition of Anasys Instruments by Bruker.

Replacing the mechanical probe of a SPM with a focused monochromatic visible light probe to detect the photothermal event created by the incident infrared radiation provides a new instrumental approach to infrared microspectroscopy. The Anasys group developed this approach and created a new company, the Photothermal Spectroscopy Corp. The company's new mIRage instrument fills the resolving power gap between FT-IR and AFM-IR. At the heart of this approach, the photon probe is focused on the sample's surface, and is coaxial and confocal with the mid-infrared radiation. This relationship is illustrated in Figure 1. The infrared source is a broadly tunable pulsed QC laser. The photothermal event, produced when the sample absorbs the infrared radiation, creates a change in the reflected or scattered light's intensity. This change in the visible light intensity is proportional to the absorption of infrared radiation used to create a photothermal infrared (O-PTIR) spectrum. The O-PTIR spectra, collected using the mIRage micro, are comparable to spectra in the KnowItAll Spectra FT-IR database (Bio-Rad). Illustrated in Figure 3, the O-PTIR spectra are well matched to the database spectra, all with a correlation factor above 98%.

With the optical probe system of the mIRage system, the resolving power in spectral imaging is improved to ~0.45 nm. Importantly, the resolving power in spectral images is limited by the wavelength of the visible-light laser and is constant across the infrared spectral range. In spectral images collected using FT-IR or QC laser micro spectrometers, the resolving power is a function of the infrared radiation, and therefore varies across the spectrum.

Operating in the noncontact reflection mode simplifies sample preparation. For example, Figure 4 shows the spectrum an individual fiber in a fabric acquired directly with no special sample preparation. Thick samples can be analyzed in the single point mode. Mapping of large areas require flat surfaces normal to incident radiation. The variety of samples, improved resolving power, quality of O-PTIR spectra and ease of sample preparation, dramatically advance microspectroscopy.

Summary

There are numerous examples of applications of infrared microspectroscopy in all academia, national laboratories, government agencies, hospitals, industries; all of them benefiting from the advances in the field (17–19). It is stimulating to see the advances of infrared microspectroscopy. The history of progress of this powerful and diverse technology is very

impressive. It is great to be part of the evolution from its humble beginnings to major factor in our growing technology. Biologists, chemists, geologists, materials scientists, microscopists, and spectroscopists around the world are awakening to the values of nanotechnology. The small world is getting larger.

References

(1) R.C. Gore, *Science* **110,** 710–711 (1949).
(2) D.D. Barer, *Nature* **163,** 198–201 (1949).
(3) V.J. Coats, A. Offner, and E.H. Siegler, *J. Optical Soc. of America* **43**(11) 984–966 (1953).
(4) F. Capasso et al., US Patent, 5,457,709, Unipolar Semiconductor Laser, 1994.
(5) F. Capasso et al., US Patent, 5,936,989, Quantum, 1997.
(6) M.S. Vitiello, *Optics Express* **23**(4), 5167–5182 (2015).
(7) K. Yeh, M. Schulmerich, and R. Bhargava, "Mid-infrared Microspectorscopic Imaging with a Quantum Cascade Laser," in *Next Generation Spectroscopic Technologies VI*, edited by M.A. Druy and R.A. Crocombe, Proc. of SPIE vol. 8726 8720E-1(2013).
(8) K. Yeh, S. Kenkel, J-N. Liu, and R. Bhargava, *Anal. Chem.* **87**(1), 485–493, (2015).
(9) H. Sreedhar, V.K. Varma, F.V. Gambacorta, G. Guzman, and M.J. Walsh, *Biomed.Opt. Express* **7**(6), 2419–2424 (2016).
(10) J.B. Bird and J. Rowlett, "A Protocol for Rapid, Label-free Histochemical Imaging of Fibrotic Liver," *Analyst* DOI:10.1039/c6an02020a (2016).
(11) C. Kuepper et al., "Quantum Cascade Laser-Based Infrared Microscopy for Label-Free and Automated Cancer Classification in Tissue Sections," *Scientific Reports*, DOI:10.1038/s41598-018-26098-w (2018).
(12) C. Prater and K. Kjoller, US Patent 8,680,467 (2013).
(13) L. Brown, M. Davanco, Z. Sun, A. Kretinin, Y. Chen, J.R. Matson, I. Vurgaftman, N. Sharac, A.J. Giles, M.M. Fogler, T. Taniguchi, K. Watanabe, K.S. Novoselov, S.A. Maier, A. Centrone, and J.D. Caldwell, *Nano Lett.* **18,** 1628–1636 (2018).
(14) F. Lu and M.A. Belkin, *Optics Express* **19**(21),19942–19947 (2011).
(15) M. Belkin, F. Lu, V. Yakolev, C. Prater, K. Kjoller, and M. Raschke, US Patent US8869602B2, High frequency deflection measurement of IR absorption (2014).
(16) F Lu, M. Jin and M.A. Belkin, *Nature Photonics* **8,** 307–312 (2014).
(17) F. Huth, Al. Govyadinov, S. Amarie, W. Nuansing, F. Keilmann, and R. Hillenbrand, *Nano Lett.* **12**(8), 3973–3978 (2012).
(18) A. Dazzi and C.B. Prater, *Chem. Rev.* **117**(7), 5146–5173 (2017).
(19) J. Chae, Qi. Dong , J. Huang, and A. Centrone, *Nano Lett.* **15**(12), 8114–8121 (2015).

John A. Reffner is a professor at John Jay College of Criminal Justice in New York, New York. Direct correspondence to: jreffner@jjay.cuny.edu

For more information on this topic, please visit: www.spectroscopymag.com/adar

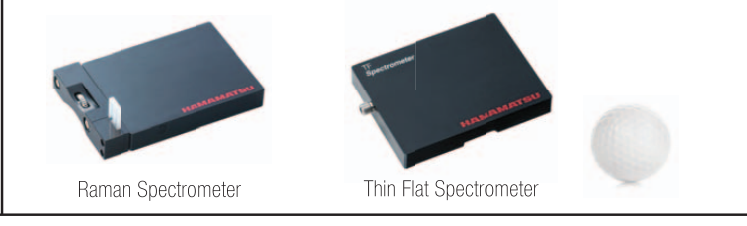

Let Hamamatsu help you find the best spectrometer for your application

Low cost NIR spectrometer
Reductions in size not performance
Ripeness, macronutrients, authentication, pathogen detection

Learn more at **www.hamamatsu.com**
Toll-free: USA 1-800-524-0504

HAMAMATSU
PHOTON IS OUR BUSINESS

Focus on Quality

A Flexible Analytical Data Life Cycle?

Does a one-size-fits-all data life cycle meet laboratory requirements for data integrity? No! The reason is that there are many different types of analytical procedures, which means that a flexible analytical data life cycle is required.

R.D. McDowall

One of the requirements of the data integrity guidances for regulated laboratories is a data life cycle that covers the birth to death of regulatory records. The data life cycle is defined in the recent MHRA data integrity guidance as "All phases in the life of the data from generation and recording through processing (including analysis, transformation or migration), use, data retention, archive/retrieval and destruction" (1).

While this is rather vague and needs a degree of interpretation, it gives an outline for a data life cycle.

A Generic Data Life Cycle, 1

After the publication of the MHRA GMP guidance in 2015 (2), I developed a data life cycle (3) that consists of two phases, active and inactive. The active phase is where most of the laboratory work occurs from acquisition to data use and short-term retention, but this is the shortest part of the life cycle. The inactive phase is where the data and records are stored for the remainder of the record retention period.

The active phase of the data life cycle consists of the following tasks:

- Data Acquisition: Controlling and recording the observation or generating data
- Data Processing: Interpretation or processing of the original data
- Generate Reportable Result: Calculation of the reportable result
- Information and Knowledge Use: Using the result to make a decision
- Short-Term Retention: Secure storage of the data and information in a secure but accessible environment for any further use—for example, audits, trending, and so on. Note that GLP requires that all study data be placed in the GLP archive at the end of the study (4,5).

The inactive phase of the data life cycle consists of the following tasks:

- Long Term Archive: The movement of the records into a secure location
- Data Migration: Migration of data from one system or repository to another over the retention period, only necessary for electronic records and not paper
- Data/Record Destruction: The formal process of destruction at the end of the retention period.

A Generic Data Life Cycle, 2

Another data life cycle interpretation was published in the GAMP Guide for Records and Data Integrity (6). This interpretation, which is consistent with the WHO data life cycle (7), defined a generic life cycle consisting of five phases:

- Creation: Acquisition of data
- Processing: Transforming and interpreting the data and calculation of the reportable result
- Review, Reporting and Use: Consisting of data review, audit trail review, data reporting, data distribution, and use of the information
- Retention and Retrieval: Covering the availability of the records, the security to ensure that unauthorized changes

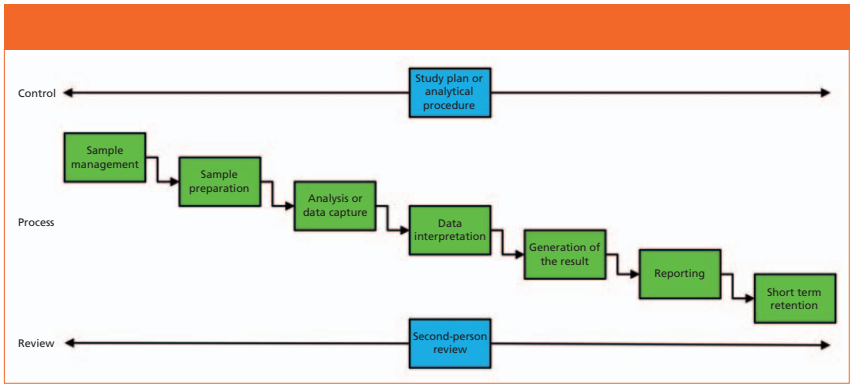

Figure 1: The active phase of an analytical data life cycle. (Adapted with permission from reference 8.)

are not made, backup and recovery, physical storage, and security and archiving, as needed
- Destruction: The formal process of destroying the records at the end of the record retention period.

My main criticism of this model is that review, reporting, and use are crammed into a single activity. Second-person review is an integral part of the creation and processing portion of laboratory work to ensure the quality and integrity of reportable results.

Generic Data Life Cycles Don't Work in the Laboratory

Generic models are good in that they provide a simple basis for understanding a data life cycle, but both models described above (3,6) may be too simplistic to apply to all situations, especially in a GXP regulated laboratory. I believe that an analytical data life cycle must be sufficiently granular for a laboratory environment. Where is sample management and sample preparation? Are these key analytical aspects all bundled into "data acquisition" or "capture"? Furthermore, where do the controlling elements of a life cycle, such as a study plan, validation plan, or analytical procedure, come into the life cycle? All are key requirements for any regulated laboratory.

I suggest that the two life cycles above are not suitable for regulated laboratories, and that an alternative approach is required.

You may think that I am being very critical of the two data life cycle models above, but if you are going to manage data integrity in a laboratory, you need to have a good understanding of each process down to a data and record level. These two models are not sufficiently detailed, and therefore we need an analytical data life cycle. The analytical data life cycle described below is essentially an expansion of the first data life cycle (3), adapted to chemical analysis.

An Analytical Data Life Cycle

The analytical data life cycle presented here still consists of two phases, active and inactive. The active phase of the analytical data life cycle, shown in Figure 1, consists of three subphases (8):
- Control: A study plan, an analytical procedure, and an analytical request that defines the work to be performed
- Process: The analytical process from sampling to reportable result
- Review: Second-person review to ensure the quality and integrity of the result.

Each task within each subphase of the life cycle will be described in more detail below.

Controlling the Analytical Data Life Cycle

In all instances, there needs to be control of the active phase of the analytical life cycle, and this control is shown in Figure 1 as either a study plan or an analytical procedure to define how work will be conducted. Even method development under the quality by design (QbD) approach advocated by the draft *USP* chapter <1220> (9) will have control by defining the analytical

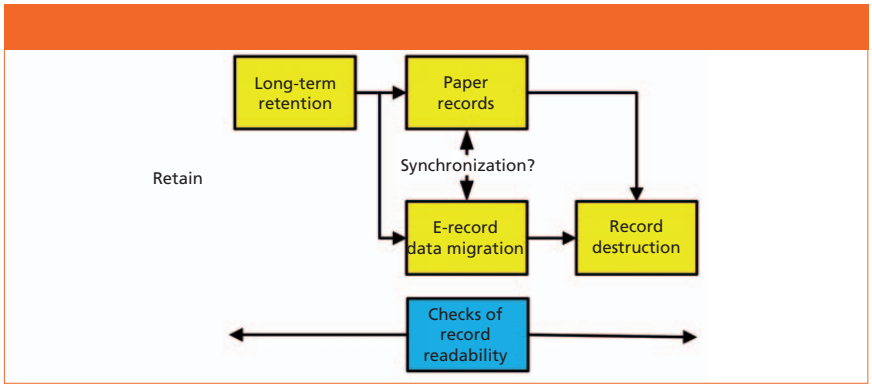

Figure 2: The inactive phase of an analytical data life cycle. (Adapted with permission from reference 8.)

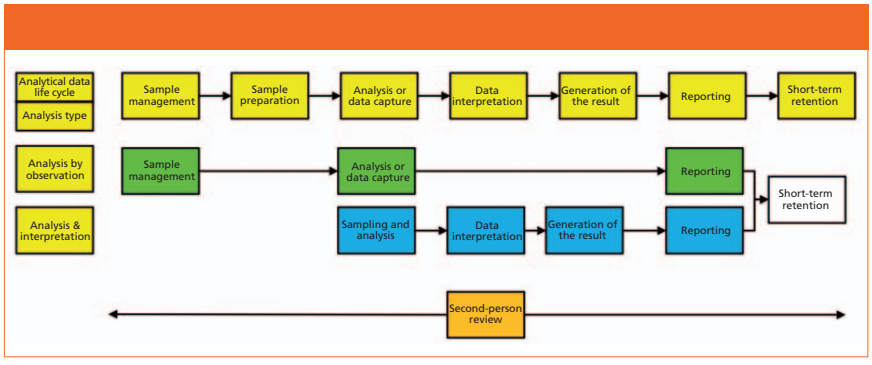

Figure 3: Different analytical procedures require a flexible analytical data life cycle. (Adapted with permission from reference 8.)

target profile (ATP) and controlling the development of a procedure. The plan or procedure must be considered as an essential part of the analytical data life cycle, because it directly determines the data that will be collected and processed. In addition to these controlling documents of the analytical life cycle, there will be standard operating procedures or work instructions for performing component tasks within the overall life cycle. These are not considered in this discussion, but are an essential part of performing and reviewing the work carried out in any analytical laboratory.

Tasks of an Analytical Data Life Cycle

In Figure 1, underneath the study plan or the analytical procedure is the main analytical data life cycle from sampling to generating reportable results. That life cycle consists of six analytical tasks together with short-term data storage.

Sample Management

Sample management covers a sampling plan, sampling process, defining the sample containers to be used, sample preservation requirements, transport, and storage in the laboratory. Because sampling is the most critical part of the analytical process, it must be performed correctly with the right documentation. The integrity of the data gathered here is essential to support the final results of the analysis and these results will include any environmental monitoring records of storage conditions during transport or storage. The major problem is that much of the sampling process is usually manual, can contain errors, and can be falsified easily. This life cycle task is not discussed in any data integrity guidance.

Sample Preparation

Preparing the samples for analysis can be as simple as transferring a liquid sample to a vessel and presenting it to an instrument, through dissolving and diluting, to complex liquid–liquid or solid-phase extraction. Although some sample preparation techniques can be automated, many of the steps are manual and typically recorded on paper. The scope of work may include preparation of reference solutions, buffers, and mobile phases using instrumentation such as sonic baths, analytical balances, pipettes, volumetric glassware, homogenizers, and pH meters. Data demonstrating that this work has been performed are essential for demonstrating both the integrity and quality of the work, including appropriate instrument calibration checks and associated instrument log book entries. Like sampling, the sample preparation task is not covered in regulatory or industry guidance documents on data integrity.

Newton and McDowall, in an article series about data integrity in the chromatography laboratory, have discussed both sampling and sample preparation in more detail for *Spectroscopy*'s sister publication, *LCGC North America* (10).

Analysis or Data Capture

The spectrum of analytical techniques applied to a sample can vary from observation (color, appearance, or odor) through wet chemistry, such as loss on drying and water content to instrumental techniques such as spectroscopy or chromatography. This task can vary from a simple observation through to the setup of a spectrometer with an appropriate software configuration to protect records, calibration, and point-of-use checks. This step is followed by the acquisition of data from the sample by following the applicable analytical procedure. The data collected here will include, as appropriate, the instrument setup, any system suitability tests or point of use checks before committing the samples for analysis, data values or data files for interpretation in the next stage of the analytical data life cycle, or just the result. Both sampling and sample preparation can be automated using either an electronic laboratory notebook (ELN) or laboratory execution system (LES).

Newton and McDowall have discussed this task in their article series on data integrity in the chromatography laboratory, but the principles described can be easily adapted for spectroscopic analysis (11).

Data Evaluation or Interpretation

In this step, the data acquired during the analysis are interpreted to obtain

processed data. Where an instrument such as a spectrometer is used, the data need to be interpreted by an analyst to obtain an identity, absorbance at a specific wavelength, or peak area counts. It may also involve the comparison of a sample spectrum with a spectral library to confirm the identity of a sample. This key task of the analytical data life cycle needs to be controlled carefully to ensure the integrity of the data. This task is also the subject of rigorous regulatory scrutiny and is the source of many data integrity citations and warning letters. This is the subject of the third part of Newton and McDowall's discourse on data integrity (12).

Generation of the Results

Following the interpretation of the data, the next task is the generation of the reportable results. This calculation can be made by a variety of means, such as manually using a calculator, using a spreadsheet, or incorporating the data into an instrument data system or other informatics application. Where possible, calculations should be performed by a validated software application, thus avoiding manual data entry. At this stage, the outliers can be identified, such as out-of-specification (OOS) results or a value on a time-versus-drug concentration curve for further investigation (OOS results, for example) (13,14).

Reporting

Following the calculation of the results, the next task in the life cycle is reporting. There are many forms that the report can take, such as a method validation or transfer report, certificate of analysis (COA), or study report. Newton and McDowall have discussed calculation of the reportable results in the fourth part of their data integrity series (13).

Second-Person Review

Before a report or COA is formally issued, the complete data package needs to be subject to a second person review. This is a critical subphase of the analytical data life cycle. The laboratory reviewer needs to be suitably trained and the review will include any instruments and computerized systems involved in the analysis. The aim of the second-person review is to ensure that the work has been carried out correctly, procedures have been followed, data have been interpreted correctly, results have been generated accurately, and the report is complete. In addition, the second-person reviewer needs to check that there have not been any data falsification or poor data management practices. The penultimate part of Newton and McDowall's series in *LCGC North America* covers the review of analytical data in more detail (15).

Short-Term Retention

Data are retained in a secure manner regardless if the records are paper or electronic. Often, the complete set of data is hybrid; consequently, there will be paper and electronic records that need to be synchronized if any changes are made after the analysis is completed and reported, such as in

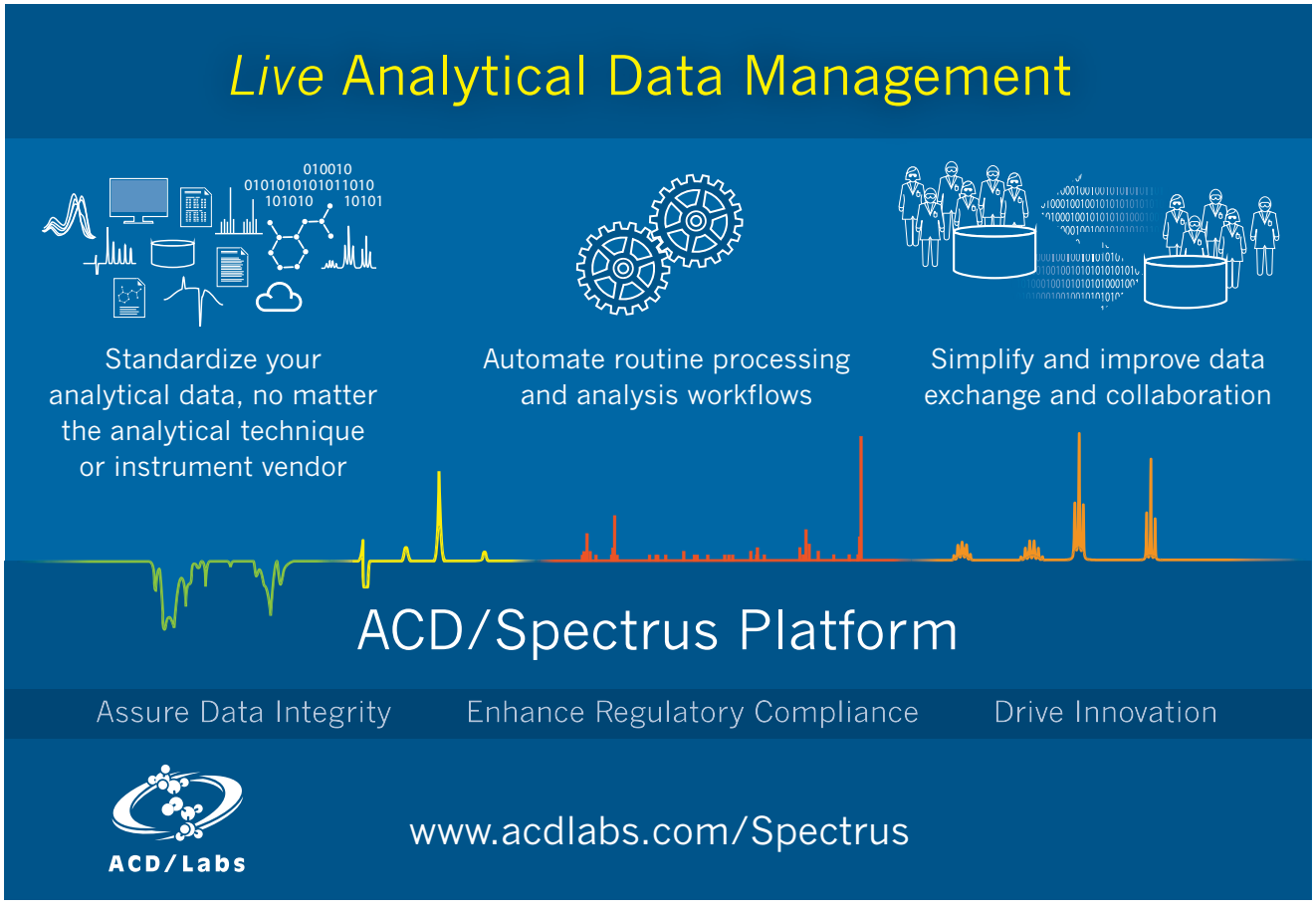

response to complaints or regulatory questions.

When the short-term data retention period has elapsed, the data are retained for the applicable retention period mandated either by the regulations or company policy.

Implicit throughout the whole of the analytical process is the applicable standard operating procedures, work instructions that describe how work should be conducted by the analytical staff. These should include how results are trended in compliance with EU GMP Chapter 6 requirements (16) and the identification of OOS or out-of-trend or out-of-expectation (OOT and OOE) results (14).

Inactive Phase

The inactive phase consists of long-term retention, possible electronic record data migration, and the destruction of the records, as shown in Figure 2. In contrast to the earlier model (3), in this model, this phase of the data life cycle (8) separates paper and electronic records. Typically, paper records are stored in an archive or record storage and are not migrated or moved during the retention period. Electronic records may have to undergo data migration during the retention period. Throughout the inactive phase, check that the records are available and can be accessed. This step applies especially to the paper and electronic records from hybrid systems, and must include the synchronization between the two media, and is the most difficult task in this phase of the life cycle.

One Analytical Size Fits All? No!

Although the analytical data life cycle in Figure 1 looks good, there is one small problem: It does not fit all analyses. The problem is that a "one-size-fits-all" approach does not work because there are many ways to analyze a sample. Therefore, this life cycle needs one more attribute to make it applicable in any regulated laboratory: flexibility. The analytical data life cycle must be able to expand and contract to fit an individual analytical process. For example:

- If a sample does not need any preparation stage before testing, will a data life cycle accommodate this situation?
- If the data acquisition is the result, why do we need the interpretation or calculation phases?

To understand this process better, look at Figure 3. This figure shows six analytical phases of the analytical data life cycle model across the top, and there are two analytical procedures modeled below it. The first is analysis by observation, where a sample is taken and the analysis is by observation of color, odor, or appearance. The observation is the reportable result which may be compared with a specification for release. The life cycle is minimal.

The second analysis shown in Figure 3 is instrumental analysis, followed by data interpretation, which is typified by near-infrared identity analysis. The sample management and sample preparation tasks of the analytical data life cycle are minimal (the number of containers to test), because the analysis is usually performed in situ in a warehouse, and the sampling and analysis phases are united in one step as the spectrum of the sample is compared to a composite spectrum in a spectral library.

Summary

As can be seen in Figure 3, an analytical data life cycle must be flexible and must be adapted to meet any analytical procedure and the data generated by it. This approach is far preferable to forcing all processes to fit a one-size data life cycle.

Acknowledgments

I would like to thank Mark Newton and Kevin Roberson for their review comments during preparation of this column.

References

(1) MHRA GXP Data Integrity Guidance and Definitions, Medicines and Healthcare Products Regulatory Agency (London, England, 2018).

(2) MHRA GMP Data Integrity Definitions and Guidance for Industry, Medicines and Healthcare Products Regulatory Agency (London, England, 2nd Ed., 2015).

(3) R.D. McDowall, *Validation of Chromatography Data Systems: Ensuring Data Integrity, Meeting Business and Regulatory Requirements (*Royal Society of Chemistry, Cambridge, UK, 2nd Ed., 2017).

(4) 21 CFR 58 Good Laboratory Practice for Non-Clinical Laboratory Studies. 1978, Food and Drug Administration: Washington, DC.

(5) OECD Series on Principles of Good Laboratory Practice and Compliance Monitoring Number 1, OECD Principles on Good Laboratory Practice. 1998, Organization for Economic Co-operation and Development, Paris, France.

(6) GAMP Guide Records and Data integrity. 2017, Tampa, FL: International Society for Pharmaceutical Engineering.

(7) WHO Technical Report Series No.996 Annex 5 Guidance on Good Data and Records Management Practices. 2016, World Health Organization: Geneva.

(8) R.D. McDowall, *Data Integrity and Data Governance: Practical Implementation in Regulated Laboratories* (Royal Society of Chemistry, Cambridge, UK, 2018).

(9) G.P. Martin et al., *Pharmacopoeial Forum,* 2017. **43**(1), (2017).

(10) M.E. Newton and R.D. McDowall, *LCGC North Am.* **36**(1), 46–51 (2018).

(11) M.E. Newton and R.D. McDowall, *LCGC North Am.* **36**(4), 270-274 (2018).

(12) M.E. Newton and R.D. McDowall, *LCGC North Am.* **36**(5), 330–335 (2018).

(13) M.E. Newton and R.D. McDowall, *LCGC North Am.* **36**(7), 458–462 (2018).

(14) FDA Guidance for Industry Out of Specification Results. 2006, Food and Drug Administration: Rockville, MD.

(15) M.E. Newton and R.D. McDowall, *LCGC North Am.* **36**(8), 527–531 (2018).

(16) EudraLex - Volume 4 Good Manufacturing Practice (GMP) Guidelines, Chapter 6 Quality Control. 2014, European Commission: Brussels, Belgium.

R.D. McDowall is the Director of RD McDowall Limited and the editor of the "Questions of Quality" column for *LCGC Europe, Spectroscopy*'s sister magazine. Direct correspondence to: SpectroscopyEdit@ubm.com

For more information on this topic, please visit our homepage at: www.spectroscopyonline.com

2019 MRS® SPRING MEETING & EXHIBIT

April 22–26, 2019 | Phoenix, Arizona

CALL FOR PAPERS

Abstract Submission Opens
September 28, 2018

Abstract Submission Closes
October 31, 2018

Spring Meeting registrations include MRS Membership July 1, 2019 – June 30, 2020

BROADER IMPACT

BI01 High Impact Practice—Increasing Ethnic and Gender Diversification in Engineering Education

CHARACTERIZATION, PROCESSING AND THEORY

CP01 Advances in *In Situ* Experimentation Techniques Enabling Novel and Extreme Materials/Nanocomposite Design
CP02 Design and *In Situ* TEM Characterization of Self-Assembling Colloidal Nanosystems
CP03 Advances in *In Situ* Techniques for Diagnostics and Synthetic Design of Energy Materials
CP04 Interfacial Science and Engineering—Mechanics, Thermodynamics, Kinetics and Chemistry
CP05 Materials Evolution in Dry Friction—Microstructural, Chemical and Environmental Effects
CP06 Smart Materials for Multifunctional Devices and Interfaces
CP07 From Mechanical Metamaterials to Programmable Materials
CP08 Additive Manufacturing of Metals
CP09 Mathematical Aspects of Materials Science—Modeling, Analysis and Computations

ELECTRONICS AND PHOTONICS

Soft Organic and Bimolecular Electronics

EP01 Liquid Crystalline Properties, Self-Assembly and Molecular Order in Organic Semiconductors
EP02 Photonic Materials and Devices for Biointerfaces
EP03 Materials Strategies and Device Fabrication for Biofriendly Electronics
EP04 Soft and Stretchable Electronics—From Fundamentals to Applications
EP05 Engineered Functional Multicellular Circuits, Devices and Systems
EP06 Organic Electronics—Materials and Devices

Semiconductor Devices, Interconnects, Plasmonic and Thermoelectric Materials

EP07 Next-Generation Interconnects—Materials, Processes and Integration
EP08 Phase-Change Materials for Memories, Photonics, Neuromorphic and Emerging Application
EP09 Devices and Materials to Extend the CMOS Roadmap for Logic and Memory Applications
EP10 Heterovalent Integration of Semiconductors and Applications to Optical Devices
EP11 Hybrid Materials and Devices for Enhanced Light-Matter Interactions
EP12 Emerging Materials for Plasmonics, Metamaterials and Metasurfaces
EP13 Thermoelectrics—Materials, Methods and Devices

ENERGY AND SUSTAINABILITY

Energy Storage

ES01 Organic Materials in Electrochemical Energy Storage
ES02 Next-Generation Intercalation Batteries
ES03 Electrochemical Energy Materials Under Extreme Conditions
ES04 Solid-State Electrochemical Energy Storage

Catalysis, Alternative Energy and Fuels

ES05 Cooperative Catalysis for Energy and Environmental Applications
ES06 Atomic-Level Understanding of Materials in Fuel Cells and Electrolyzers
ES07 New Carbon for Energy—Materials, Chemistry and Applications
ES08 Materials Challenges in Surfaces and Coatings for Solar Thermal Technologies
ES10 Rational Designed Hierarchical Nanostructures for Photocatalytic System
ES11 Advanced Low Temperature Water-Splitting for Renewable Hydrogen Production via Electrochemical and Photoelectrochemical Processes
ES12 Redox-Active Oxides for Creating Renewable and Sustainable Energy Carriers

Water-Energy Materials and Sustainability

ES09 Advanced Materials for the Water-Energy Nexus
ES13 Materials Selection and Design—A Tool to Enable Sustainable Materials Development and a Reduced Materials Footprint
ES14 Materials Circular Economy for Urban Sustainability

Photovoltaics and Energy Harvesting

ES15 Fundamental Understanding of the Multifaceted Optoelectronic Properties of Halide Perovskites
ES16 Perovskite Photovoltaics and Optoelectronics
ES17 Perovskite-Based Light-Emission and Frontier Phenomena—Single Crystals, Thin Films and Nanocrystals
ES18 Frontiers in Organic Photovoltaics
ES19 Excitonic Materials and Quantum Dots for Energy Conversion
ES20 Thin-Film Chalcogenide Semiconductor Photovoltaics
ES21 Nanogenerators and Piezotronics

QUANTUM AND NANOMATERIALS

QN01 2D Layered Materials Beyond Graphene—Theory, Discovery and Design
QN02 Defects, Electronic and Magnetic Properties in Advanced 2D Materials Beyond Graphene
QN03 2D Materials—Tunable Physical Properties, Heterostructures and Device Applications
QN04 Nanoscale Heat Transport—Fundamentals
QN05 Emerging Thermal Materials—From Nanoscale to Multiscale Thermal Transport, Energy Conversion, Storage and Thermal Management
QN06 Emerging Materials for Quantum Information
QN07 Emergent Phenomena in Oxide Quantum Materials
QN08 Colloidal Nanoparticles—From Synthesis to Applications

SOFT MATERIALS AND BIOMATERIALS

SM01 Materials for Biological and Medical Applications
SM02 Progress in Supramolecular Nanotheranostics
SM03 Growing Next-Generation Materials with Synthetic Biology
SM04 Translational Materials in Medicine—Prosthetics, Sensors and Smart Scaffolds
SM05 Supramolecular Biomaterials for Regenerative Medicine and Drug Delivery
SM06 Nano- and Microgels
SM07 Bioinspired Materials—From Basic Discovery to Biomimicry

www.mrs.org/spring2019

Meeting Chairs

Yuping Bao The University of Alabama
Bruce Dunn University of California, Los Angeles
Subodh Mhaisalkar Nanyang Technological University
Ruth Schwaiger Karlsruhe Institute of Technology—Institute for Applied Materials
Subhash L. Shinde University of Notre Dame

Don't Miss These Future MRS Meetings!

2019 MRS Fall Meeting & Exhibit
December 1–6, 2019, Boston, Massachusetts

2020 MRS Spring Meeting & Exhibit
April 13–17, 2020, Phoenix, Arizona

MRS MATERIALS RESEARCH SOCIETY®
Advancing materials. Improving the quality of life.
506 Keystone Drive • Warrendale, PA 15086-7573
Tel 724.779.3003 • Fax 724.779.8313 • info@mrs.org • www.mrs.org

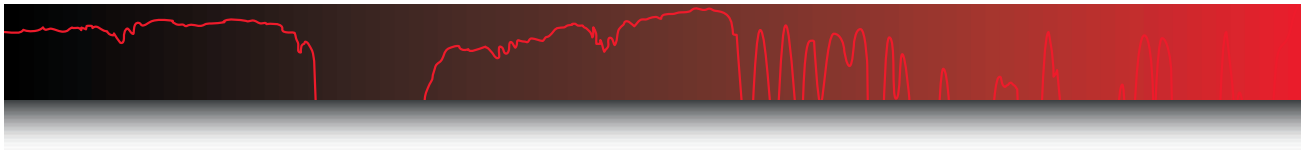

IR Spectral Interpretation Workshop

The C=O Bond, Part VII: Aromatic Esters, Organic Carbonates, and More of the Rule of Three

In this seventh installment of our study of the infrared spectroscopy of the carbonyl group, we look at aromatic esters and carbonates. We see that aromatic esters follow the ester Rule of Three, but that each of these three peak positions is different for saturated and aromatic esters, which makes them easy to distinguish. Organic carbonates are structurally similar to esters and follow their own Rule of Three.

Brian C. Smith

In our last installment (1), I introduced you to the ester functional group. As a review, the molecular structure and the naming of the atoms in an ester group are shown in Figure 1.

Recall that there are two types of esters, depending on the identity of the alpha carbon. If the alpha carbon is saturated, the ester is saturated. If the alpha carbon is aromatic, the ester is aromatic. In the last column, I only had room for a discussion of saturated esters. In this installment, we will finish our discussion of esters by covering aromatic esters.

Organic carbonates as a functional group are similar to esters, and so it is appropriate to group them with aromatic esters. The chemical term *carbonate* is a little confusing. There exist inorganic carbonates that contain the CO_3^{2-} ion. Although this functional group contains a carbon atom, it acts inorganic, since it forms ionic bonds and makes up rocks such as limestone, rather than typical organic compounds. Organic carbonates also contain a carbon atom with three oxygens bonded to it, but the bonding is covalent, and the functional group is considered organic. Therefore, it is always important to use the term *organic carbonates* when discussing the covalent version of this moiety.

Structurally, organic carbonates look like two esters squished together, as is shown in Figure 2.

As you can see in Figure 2, carbonates are symmetrical, and each half can be thought of as an ester, with each half having a carbonyl carbon, an ester oxygen, and an alpha carbon. Note that the carbonyl carbon has not one oxygen attached to it, as in an ester, but two. This means there are two ester oxygens and two alpha carbons. There are three types of carbonates: saturated, where both alpha carbons are saturated, aromatic, where both alpha carbons are aromatic, and mixed, where one alpha carbon is saturated and one is aromatic. Given the structural similarity between esters and organic carbonates, we might expect them to follow the Rule of Three, and as we will see they do. As we will also see, we can distinguish between the three types of carbonates based on their infrared spectra, and, in general, distinguish between esters and carbonates based on their spectra.

The Infrared Spectroscopy of Aromatic Esters

In the last column (1), we saw that esters have a memorable pattern of three intense peaks at ~1700, ~1200, and ~1100 from the

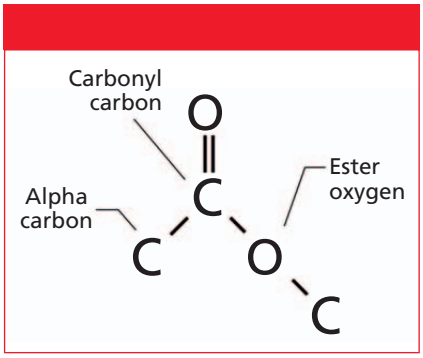

Figure 1: The molecular structure of the ester functional group.

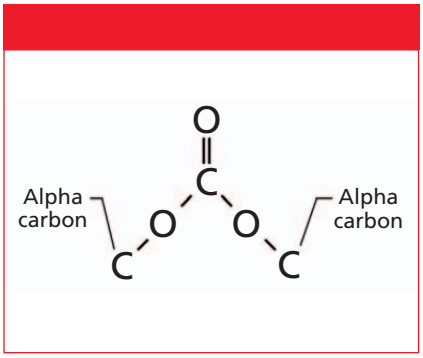

Figure 2: The molecular framework of an organic carbonate.

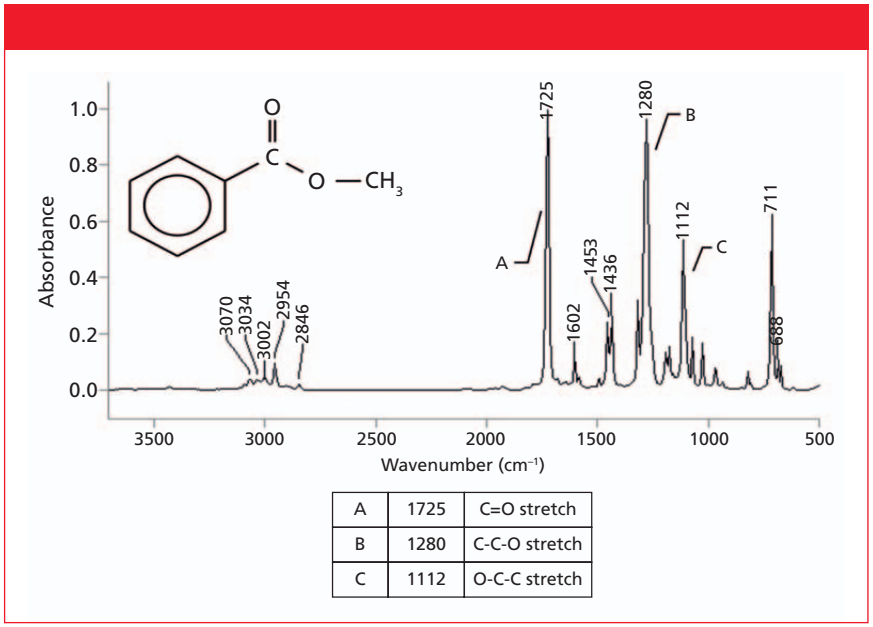

A	1725	C=O stretch
B	1280	C-C-O stretch
C	1112	O-C-C stretch

Figure 3: The infrared spectrum of methyl benzoate, an aromatic ester.

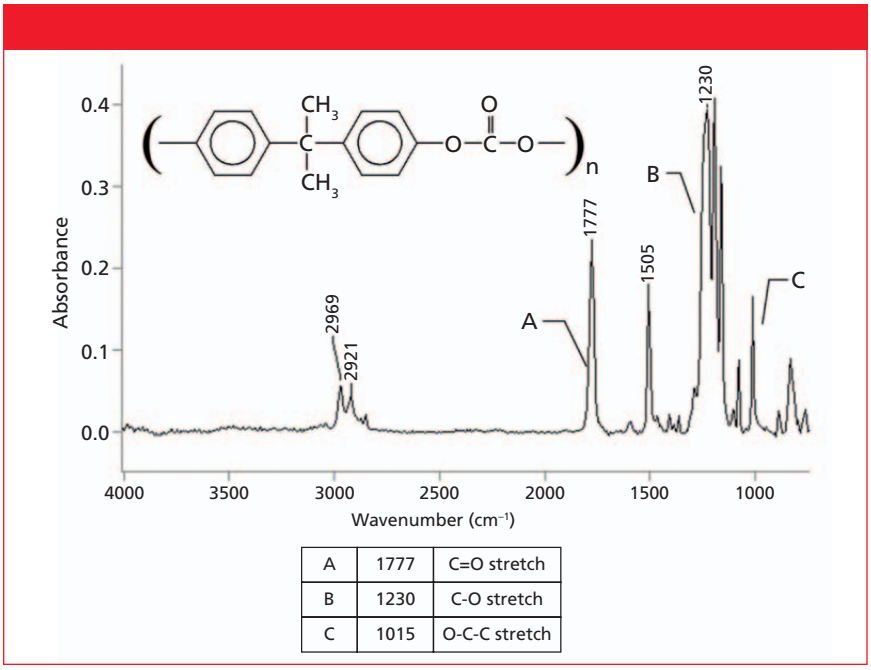

A	1777	C=O stretch
B	1230	C-O stretch
C	1015	O-C-C stretch

Figure 4: The infrared spectrum of the aromatic carbonate Lexan.

art photonics
Broad Spectra Optical Fiber Solutions

Fiber probes for any spectroscopy method used in 0.2-16µm range for clinical diagnostics

visit us at:
artphotonics.com

Quiz Section: Answer to the July Quiz and a New Interpretation Challenge

The Last Quiz

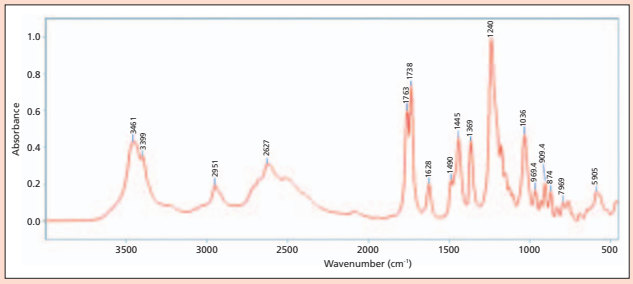

Figure *i*: The problem spectrum from the last installment.

Table *i*: Peak positions for the last installment's spectral interpretation challenge		
3431, 3391	1763, 1738	1240
2951	1490, 1445	1036
2700–2400	1369	

Figure *i* shows the problem infrared spectrum from the last column. Your task was to determine the whether this compound contains an ester, and, if so, what type. Table *i* shows the relevant peak positions. I also mentioned that this is the spectrum of a notorious controlled substance.

Remembering that the first of the Rule of Three peaks is a C=O stretch, the first place you should look to solve this problem is between 1800 to 1600, where carbonyl groups absorb. There are two large peaks here at 1763 and 1738. We learned in the last column that saturated esters have a C=O stretch from 1750 to 1735. The peak at 1738 is a candidate to be this. The next thing to do is to find the C-C-O stretch, the second of the Rule of Three peaks. For saturated esters, this peak typically falls from 1210 to 1160. There is no peak in this range in Figure *i*. However, there is a huge peak at 1240, which is, in fact, the biggest peak in the spectrum. Recall (1) that acetate esters have a special high wavenumber C-C-O stretch that falls at ~1240. This peak is certainly that, indicating not only that we have a saturated ester, but that it is an acetate. Lastly, the O-C-C stretch for saturated esters is found between 1100 and 1030. The peak at 1036 fits the bill here. Therefore, we have a saturated ester as identified by its Rule of Three peaks: the C=O stretch at 1738, the acetate C-C-O stretch at 1240, and the O-C-C stretch at 1036.

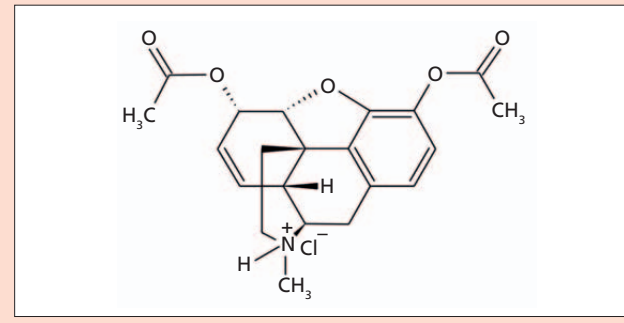

Figure *ii*: The molecular structure of heroin hydrochloride hydrate.

The acetate ester we discovered is part of the structure of the notorious controlled substance heroin. This spectrum is in fact that of heroin hydrochloride hydrate, the structure is of which shown in Figure *ii*.

Note that there are not one but two acetate groups in heroin, which is why the acetate C-C-O stretch at 1240 is so intense. The two carbonyl stretching peaks at 1768 and 1735 are a bit confusing. I believe they are both from the acetate groups, and they are different because the acetates are attached to different parts of the molecule.

Your Next Infrared Spectral Interpretation Challenge

Using everything you have learned in this and previous columns, determine the functional groups present and try to discover the chemical structure of this compound. Remember that inclusion of a peak position in the table does not necessarily mean that it will be useful in the structural determination.

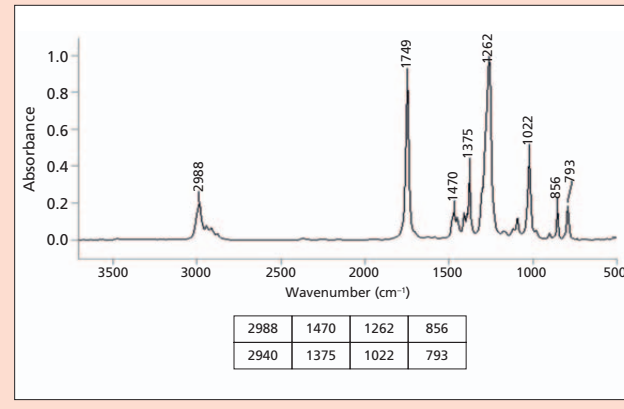

2988	1470	1262	856
2940	1375	1022	793

Figure *iii*: The infrared spectrum of a solid.

C=O and two C-O stretches, and hence follow what I call the Rule of Three (2). We also saw that saturated esters follow the Rule of Three. Aromatic esters also follow the Rule of Three, but all three peaks for aromatic esters fall in different wavenumber ranges than the peaks of saturated esters do (Figure 3).

The Rule of Three peaks in Figure 3 are labeled A, B, and C, and are easy to spot, sticking up like three long fingers in the middle of the spectrum. The peak labeled A at 1725 is the unmistakable C=O stretch, and is almost always the most intense peak in the spectrum. In general, for aromatic esters this peak falls between 1730 and 1715, and is lower than that of saturated esters because of conjugation (1). Peak B at 1280 is the C-C-O stretch, which is normally found from 1310 to 1250. Lastly, peak C is the O-C-C stretch, which ranges from 1130 to 1100. These three peaks follow the intensity pattern we have

> COMING TOGETHER is a BEGINNING; KEEPING TOGETHER is PROGRESS; WORKING TOGETHER is SUCCESS

THANK YOU for making this the largest Cannabis Science Conference ever! We never dreamed of having over 2,500 attendees and 160 sponsors/exhibitors at our third conference! Together we are advancing cannabis science, and who knew that doing the impossible could be so much fun!

- Josh Crossney
President, CSC Events, LLC

CSC Events, LLC, is small team, but we are dedicated to hosting truly spectacular events. Our team has created many interesting and innovative additions, from the Canna Boot Camp pre-conference workshop to exciting, interactive panels. We are devoted to serving our customers and providing a conference experience with maximum impact and networking.

(CSC Events, LLC, team pictured with Montel Williams, our 2017 plenary speaker.)

SAVE THE DATES!!!

2019 CANNABIS SCIENCE CONFERENCE

SEPTEMBER 4-6

OREGON CONVENTION CENTER

CannabisScienceConference.com

EXHIBITORS: Sign up within the next 30 days and receive 10% off!

Table I: The Rule of Three peak positions for saturated and aromatic esters

Vibration	Saturated Esters	Aromatic Esters
C=O stretch	1750–1735	1730–1715
C-C-O stretch	1210–1160	1310–1250
O-C-C stretch	1100–1030	1130–1100

Table II: The Group wavenumbers of organic carbonates

Vibration	Saturated Carbonates	Mixed Carbonates	Aromatic Carbonates
C=O stretch	1740 ± 10	1790–1760	1820–1775
O-C-O stretch	1280–1240	1250–1210	1230–1205
O-C-C stretch	1060–1000	1060–1000	1060–1000

seen before for esters, where the first two Rule of Three peaks are more intense than the third. Table I lists the Rule of Three peak positions for aromatic esters, and compares them to those for saturated esters.

Note in Table I that, for each of the three vibrations listed, the ranges for saturated and aromatic esters are different. Each ester type has a unique set of Rule of Three peaks, and any of the peaks can be used to distinguish saturated and aromatic esters from each other.

The Infrared Spectra of Organic Carbonates

As discussed above, organic carbonates come in saturated, aromatic, and mixed forms. The infrared spectrum of an aromatic carbonate, the common polymer Lexan (2,2-bis[4-hydroxyphenyl]propane polycarbonate), is shown in Figure 4.

Lexan is an aromatic carbonate because the two alpha carbons are part of benzene rings. The peak at 1777 is undoubtedly a C=O stretch based on its strength and position. The carbonyl stretch of aromatic carbonates in general falls from 1820 to 1775. This region is higher than that of any ester, and makes it easy to distinguish between aromatic esters and carbonates. The C=O stretch of mixed carbonates falls from 1790 to 1760, and for saturated carbonates this peak is seen at 1740 ± 10.

Esters have a C-C-O stretch that falls around 1200 (1). Carbonates have instead have an O-C-O bond, and the asymmetric stretch of this bond is seen at 1230 in Figure 4. For mixed carbonates, it falls from 1250 to 1210, and, for saturated carbonates, from 1280 to 1240. Lastly, carbonates contain an O-C-C moiety whose asymmetric stretch can be seen at 1015 in Figure 4. This peaks falls between 1060 and 1000 for all types of carbonates.

To review, then, carbonates follow the Rule of Three like esters with three intense peaks at ~1700, 1200, and 1000. These peaks are from the C=O, O-C-O, and O-C-C stretches. The first two are sensitive to the type of carbonate; the O-C-C stretch is not. A summary of the group wavenumbers for organic carbonates is shown in Table II. Note that the saturated carbonate C=O stretch falls in the same range as that of saturated esters (Table I). However, saturated carbonates have their O-C-O peak from 1280 to 1240, whereas for saturated esters, the C-C-O peak is lower, from 1210 to 1160. It is the relative position of these two peaks that allows one to distinguish saturated esters and carbonates from each other. The high-wavenumber C=O stretches of mixed and aromatic carbonates mean they will never be confused with esters.

Conclusions

Like saturated esters, aromatic esters follow the Rule of Three with intense peaks at ~1700, 1200, and 1100 from C=O, C-C-O, and O-C-C stretches. However, as shown in Table I, saturated and aromatic esters have unique Rule of Three peaks, and any of these peaks can be used to distinguish these two types of esters from each other.

Carbonates are similar structurally to esters and also follow their own Rule of Three with peaks from C=O, O-C-O, and O-C-C stretches. Carbonates can be distinguished from esters and each other using the peaks listed in Table II.

References

(1) B.C. Smith, *Spectroscopy* **33**(7), 20–23 (2018).
(2) B.C. Smith, *Infrared Spectral Interpretation: A Systematic Approach* (CRC Press, Boca Raton, Florida, 1999).

Brian C. Smith, PhD, has more than three decades of experience as an infrared spectroscopist. He has published numerous peer reviewed papers and has written three books on the subject: *Fundamentals of FTIR* and *Infrared Spectral Interpretation*, both published by CRC Press, and *Quantitative Spectroscopy: Theory and Practice* published by Elsevier. As a spectroscopy trainer, he has helped thousands of people around the world improve their infrared analyses. He earned his PhD in physical chemistry from Dartmouth College. He can be reached at: SpectroscopyEdit@UBM.com

For more information on this topic, please visit our homepage at: www.spectroscopyonline.com

CONNECT WITH SPECTROSCOPY ON SOCIAL MEDIA

Join your colleagues in conversation, respond to hot topic questions, and stay up-to-date on breaking news. "Like" and follow us on Twitter, LinkedIn, and Facebook today!

Spectroscopy®

www.spectroscopyonline.com/SpecConnect

SARUNYU_FOTO / SHUTTERSTOCK.COM

Identification of Graphite Mechanical Behavior and Dislocations by Micro-Raman Microscopy

Using micro-Raman microscopy, we examine graphite mechanical behavior through the evolution of dislocation defect density and the resultant deformation (strain) in graphite components. The strengthening of the Raman-active G and D phonon modes observed in the Raman spectrum under loading condition is attributed to an increase in the number of dislocations in the graphite structure. The increasing strength of the Raman optical phonon modes linked with a generous number of dislocations indicates the potential capability of the Raman spectroscopy technique to help develop a mechanistic understanding of the complex mechanical behavior of graphite for use in many industries and applications. The identification of deformation behavior and a dislocation-mediated deformation process in graphite is the ultimate aim of our research as well as to develop a better understanding of the graphite mechanical behavior, which is important to clean nuclear fission energy technologies.

Ram Krishna and Paul M. Mummery

Graphite is a potential material for the development of next-generation nuclear energy systems (1). The physical processes characterizing the failure of graphite structures require experimental insights to describe nucleation and propagation of dislocations and their interaction. There is little data describing the physical mechanisms responsible for initiating failure in graphite. The aim of this research is to explore the Raman spectroscopy and microscopy techniques to better understand how dislocations deform the bulk crystals associating to the graphite mechanical behavior and the way graphite structure accommodates the strain before failure. The developed technique is used for graphite materials to quantify dislocation density in the structure derived from the strengthening and shifting of Raman peaks dependent on the loading conditions. The applied external stress involves the start of movement of the existing dislocations, the generation of new dislocations, and the subsequent interaction among them through the Frank-Read mechanism (2). The motion and interaction of dislocations tend to happen on available slip planes along various directions in a hexagonal crystal system for components failure (3).

The progressive evolution of dislocations in graphite bulk crystals leads to little gross plastic deformation before failure under externally applied stresses. At a microscopic level, deformation resulting from cumulative movement of dislocations involves cracking and reformation of interatomic carbon bonds, contributing to the Raman D-peak. The characteristic nature of dislocation motion in specific directions and planes provides deformation of components. The existing dislocations and defects, crystal boundaries, cracks, and pores in the structure are important in initiating and propagating deformation and a potential reason for a dramatic increase in the number of dislocations and growth of preexisting cracks.

Experimental

Materials and Compression Test

A distinct laminar structure of graphite composed of a two-dimensional (2D) material known as graphene. The layered structure is constituted of basal planes where strong sp^2-hybridized carbon atoms form hexagons in a honeycomb structure. The basal layers are held together through weak interlayer dispersion forces. The weak inter-

layer forces allow the crystallographic graphitic planes to adiabatic shear over each other, promoting the crystallographic defects in the bulk of crystals while maintaining the sp^2 connectivity. Samples of graphite grade that are suitable for nuclear energy applications were used for the present study.

Quasistatic compression tests were conducted using a 5KN Deben Micro tester (Deben UK Ltd.). A miniature compression stage specifically designed to test microcomponents and a real-time observation of compressed region of a test sample were used under micro-Raman microscopy's enclosure. Compression tests were performed at ambient temperature inside the Raman spectrometer enclosure using a controlled load cell by an external controlling unit through electronic cabling.

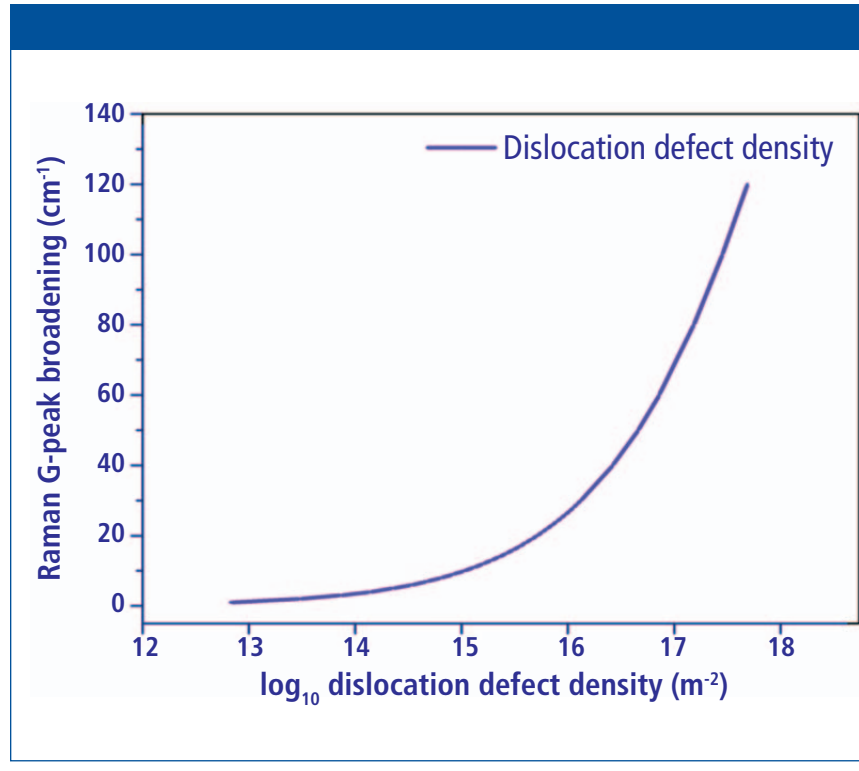

Figure 1: Calibration of the Raman G-peak broadening as a function of dislocation density in graphite predicted from a physical model based on graphite material properties. Adapted with permission from reference 3.

Raman Microscopy

Raman spectroscopy has been considered as an effective technique to non-

ONDAX
RAMAN SPECTROSCOPY PRODUCTS
See what you've been missing with THz-Raman®
Structural Fingerprint
Chemical Fingerprint
Carbamazepine
Form 2
Form 3
Structural Fingerprint Clearly Identifies Polymorphs
Raman Signal (a.u.)
Raman Shift (cm-1) [THz]
Both Stokes and anti-Stokes signals down to 5cm-1
Complete chemical fingerprint
THz-Raman®
Ultra-low Frequency THz-Raman® Systems & Accessories
High Throughput Screening
In-situ Process Probes
Transmission Mode for Bulk Testing
Microscope/ Benchtop
CleanLine™
SureLock™
Specializing in low-frequency Raman Systems and Components
Wavelength Stabilized and Single Frequency Lasers from 405nm to 1064nm
ASE FREE MODULES
MINI-BENCHTOP
TURNKEY MODULES
OEM SOLUTIONS
COMPONENTS
ONDAX Online Store
Advanced Solutions for Optical Measurements
850 E. Duarte Rd. Monrovia, CA 91016
T. 626.357.9600 (Tel) | F. 626.513.7494 | sales@ondax.com
© 2018 Ondax, Inc.

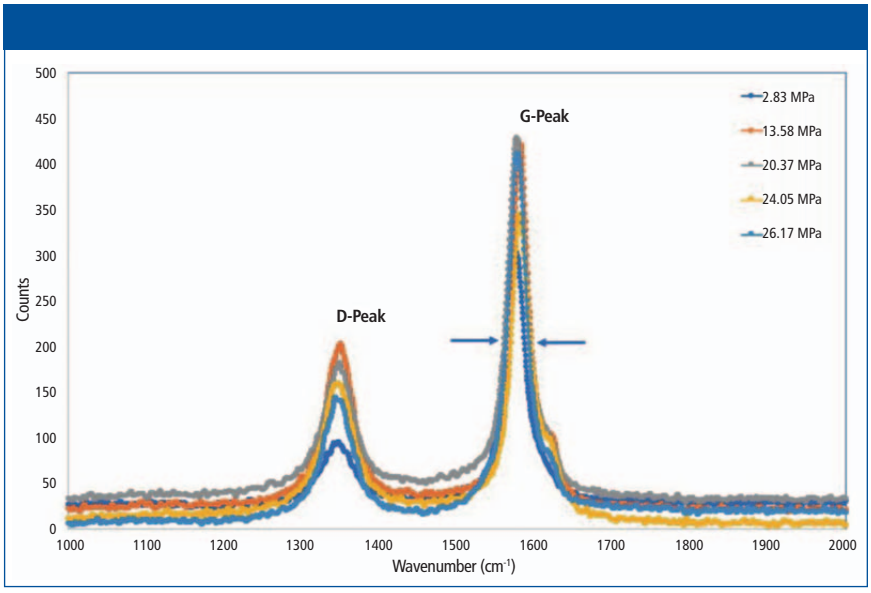

Figure 2: Evolution of Raman spectrum under applied external stresses. Applied external stress increases the FWHMs of the Raman peaks (D and G) (shown by arrows), which are linked to dislocation density accumulation and generation of micro-cracking in the structure.

Table I: Raman spectral analysis for graphite deformation behavior

Stress (MPa)	2.83	13.58	20.37	24.05	26.17 (failure stress)
Raman G-peak (cm^{-1})	1578.0	1576	1577	1579.5	1580
Raman G-width (FWHM)	28.33	30.53	32.76	32.93	36.95
Dislocation density [$\times 10^{15}$] (m^{-2})	9.62	12.8	16.5	16.8	24.7
A_D/A_G (integral area ratio)	0.55	0.637	0.689	0.726	0.779
In-plane crystallite size, L_a (nm)	34.43	30.20	27.9	26.49	24.68

destructively evaluate local internal stresses (4) and material structural changes in graphite (5). Moreover, any disorder in the spatial arrangement of sp^2-hybridized carbons in hexagonal rings and the optical phonon dispersion of graphite provide information in the Raman spectra that could be used to derive failure property of a component (6).

Raman spectra of carbon and its derivatives are well documented in the literature. The sp^2-bonded carbons exhibit symmetry allowed by the E_{2g} first-order graphite (G) band at a wavenumber of 1580 cm^{-1} and a disorder-induced (D) A_{1g} band at a wavenumber of 1350 cm^{-1}. First-order Raman spectra are commonly used to characterize defect and disorder in graphite microstructure (7).

Micro-Raman spectroscopy was conducted using a Senterra Raman microscope (Bruker Optics, Inc.), with a 532-nm wavelength excitation laser in a confocal mode of operation at a spatial resolution of 0.8 µm.

Results and Discussion

The strengthening of the Raman G-peak in stressed graphite is linked to the dislocation population in the structure over the scanned volume, which resulted in a strained crystallite region. To quantify the number of dislocations introduced in the structure, a physical model is developed and detailed methodology is provided in the literature (3). Figure 1 shows the calibration of Raman G-peak broadening as a function of dislocation population in graphite predicted using the model based on graphite physical properties (3,4).

The deformation strains concomitant with Raman G-peak shift (4) and their quantification is relatively straightforward for a known grain orientation, although the process is cumbersome for an arbitrary grain orientation. It may provide a wrong interpretation if grain orientation information is neglected. Therefore, it is essential before the measurement to know what the grain orientation in the component is. In the present work, we used a known grain orientation of polycrystalline graphite developed during the manufacturing process, marked as axial, radial, and azimuthal directions.

The graphite deformation behavior information derived from the Raman data is shown in Table I. The full width half maximum (FWHM) of the G-peak strengthened during loading conditions, and the Raman spectra have been analyzed to quantify the crystallite lateral size and dislocation density for each loading condition. The derived dislocation data at different stress values (Table I) show a nonlinear trend. Dislocations in the graphite microstructure in preexisting conditions (before the application of loading) was 7.5 x 10^{14} m^{-2}. It is important to note that continuous increases in the dislocation population in the elastic region and further increases of dislocations and microcrack formation in the plastic deformation region are connected to stress increments (8).

Figure 2 shows Raman spectra indicating D and G peaks with an increase in applied external stresses. The applied external stresses develop a strained crystallite region and are characterized by the changes in the Raman phonon frequencies as the carbon–carbon bonding lengths and angles alter as a material response to the straining effect.

Quantification of dislocation density reveals that stresses imposed on the structure increases dislocation interaction and reach a sufficiently high value before failure (Table I). The calibration data shows that dislocations do not appear to saturate at high G-peak broadening (Figure 1), which indicates that during deformation a relative shearing of basal layers in an organized manner is a prominent process for generating dislocations.

An increase in applied stress results in cumulative movement of dislocations, subsequently developing a plastic deformation in the structure. It is well known that slip directions and slip planes are important to know for a crystal system because edge dislocations move by slip and climb while screw dislocations can be moved by slip or cross-slip. The onset of deformation involves the motion of dislocations where they interact among themselves. Dislocation interaction is very complex depending on the number of slip planes available and for a hexagonal system only a limited number of slip planes exists. For example, in a hexagonal crystal system, the basal plane is the most common slip plane and prismatic or pyramidal planes are less common slip occurrence planes. In both slip planes, close packed directions are the slip directions.

Dislocations either annihilate or repel depending on their nature and subsequently affect the strain energy of accommodating material. A large fraction of dislocations do not annihilate completely because they are situated on neighboring slip planes, resulting in the formation of a row of vacancies or interstitial atoms. The hindrances to dislocation motion include crystallite boundaries, pores, cracks and change in the structure because of crystallographic orientation or phase change (binder to filler or vice-versa). The consequence of these hindrances of dislocation motion is the movement of dislocations at higher stresses. Dislocation can generate from preexisting dislocations, defects, disorder, crystallite boundaries, and surface irregularities. Because of the presence of these imperfections in abundance in graphite, the dislocation population dramatically increases during the onset of plastic deformation. Because further motion of dislocations requires an increase in stress, crossing the yield stress of material and reaching an ultimate strength before failure occurs. Therefore, a nonlinear relationship between Raman peaks and graphite microstructural information was observed. Graphite is a polycrystalline material and plastic deformation corresponds to distortion of the individual crystallites by means of slip. Further, note that in polycrystalline material crystallites may or may not be favorable for slip and each crystallite provides a mutual geometrical constraint on one other. Therefore, plastic deformation does not exist at low applied stresses and to initiate plastic deformation, a higher stress is required depending upon the orientation of crystallites. According to von Mises criterion, a minimum of five independent slip systems must be operative to maintain crystal boundary integrity and exhibit ductile behavior, which is not the case for most hexagonal crystal systems and graphite material. Therefore, polycrystalline graphite never shows ductile behavior, although small plastic deformation may be noticeable because of twinning or a favorable preferred orientation (9).

Understanding the graphite deformation behavior through the capability of the Raman technique provides a better insight about the deformation physical processes characterizing crack initiation, propagation, and subsequent failure. Raman spectral analysis shows an increase in the concentration of dislocation with a reduction in graphite crystal size (see Table I). The orientations of crystallites are mostly misaligned and thus, it is difficult for a dislocation moving on a common slip plane in one crystallite to pass over to a similar slip plane in another crystallite. In addition, the crystallites are separated by a thin noncrystalline region, which is the characteristic of a crystal boundary. Such atomic disorder at the boundary causes discontinuity in the slip planes. The smaller the crystallite size, the more frequent the pile up of dislocations is. Hence, dislocations are stopped by a crystal boundary, pile up against it, and show a rise in the ultimate stress.

Concluding Remarks

Raman microscopy is a reliable, fast, and sensitive technique for monitoring graphite deformation behavior and in the present research a practical application of the deformation behavior was discussed. This material information is of great importance from a point of fracture and in terms of gaining knowledge of the characteristic property of materials. The development in modern optics including diode lasers, improved detector capabilities, and fiber-optic coupling have led to a rapid increase in the use of the Raman technique, and it is gradually becoming a mature technique.

References

(1) T.R. Allen, K. Sridharan, L. Tan, W.E. Windes, J.I. Cole, D.C. Crawford, and G.S. Was, *Nucl. Technol.* **162**(3), 342–357 (2008).

(2) B. Kelly, *Physics of Graphite* (Applied Science Publishers, London, 1981).

(3) R. Krishna, J. Wade, A.N. Jones, M. Lasithiotakis, P.M. Mummery, and B.J. Marsden, *Carbon* **124**(Supplement C), 314–333 (2017).

(4) R. Krishna, A.N. Jones, R. Edge, and B.J. Marsden, *Radiat. Phys. Chem.* **111,** 14–23 (2015).

(5) R. Krishna, T.J. Unsworth, and R. Edge, *Materials Science and Materials Engineering* (Elsevier, 2016).

(6) M.A. Pimenta, G. Dresselhaus, M.S. Dresselhaus, L.G. Cancado, A. Jorio, and R. Saito, *Phys. Chem. Chem. Phys.* **9**(11), 1276–1290 (2007).

(7) A.C. Ferrari, *Solid State Commun.* **143**(1), 47–57 (2007).

(8) T. Oku, T. Usui, M. Eto, and Y. Fukuda, *Carbon* **15**(1), 3–8 (1977).

(9) J.F. Nye, *Physical Properties of Crystals: Their Representation by Tensors and Matrices* (Oxford University Press, Great Britain, 1985).

Ram Krishna and P**aul M. Mummery** are with the Nuclear Graphite Research Group, School of Mechanical, Aerospace & Civil Engineering, at The University of Manchester in Manchester, UK.
Direct correspondence to:
ram.krishna-2@manchester.ac.uk ■

For more information on this topic, please visit our homepage at: www.spectroscopyonline.com

Infrared Spectroscopy: New Frontiers Both Near and Far

Until very recently, the conventional optical resolution limits for far-field infrared (IR) imaging were ~5–10 µm, given the 2–25 µm wavelengths and the typical optics of mid-IR microscopes. In 2011, the diffraction limit for far-field IR was achieved with synchrotron source light, high numerical aperture (NA) optics, and a focal plane array detector. Comparable capability for thermal-source IR microscopes is now commercially available. Single-wavelength scanning, with quantum cascade lasers, and fast, full spectrum imaging, with focal plane array detectors, permit collection of infrared images on samples with dimensions on the order of centimeters, within minutes. Near-field IR techniques embody a conceptual paradigm shift, preserving the analytical power of IR spectroscopy, while breaking the diffraction limit constraints for a 100-fold improvement in spatial resolution. Exploration of the chemistry of materials at micrometer and nanometer scales leads to a better macroscopic perspective, as illustrated here with examples from our ongoing research in materials, environmental, and biomedical applications.

Negar Atefi, Tanvi Vakil, Zahra Abyat, Sarvesh K. Ramlochun, Gorkem Bakir, Ian M.C. Dixon, Benedict C. Albensi, Tanya E.S. Dahms, and Kathleen M. Gough

Infrared (IR) spectroscopy has been a reliable workhorse in research, industry, and education for many decades. The basic principles are well understood (1), and are embedded in various ways through commercial and in-house designed instruments. Whether acquired in transmission or transflection, attenuated total internal reflection, diffuse reflectance, or grazing angle incidence, in bulk, or through an infrared microscope, the strengths and weaknesses have been well defined for decades. Recently, several transformative conceptual breakthroughs and innovations that work beyond the traditional instrumental designs have opened up exciting new avenues for application.

In far-field IR spectromicroscopy, imaging and even oversampling relative to the diffraction limit was only achieved in 2011 (2). Despite these advances, all IR spectromicroscopy has been subject to the fundamental physical limitations of diffraction; to be specific, the inescapable fact that the size and separation of resolvable features is directly proportional to the IR wavelengths, at best ~1 µm for the OH, NH stretch region, and 3–5 µm for the fingerprint region. The transformative breakthrough of near-field IR is based on coupling the nanoscale focus of atomic force microscopy with infrared illumination. In my laboratory, we have applied some of these new techniques to imaging of heterogeneous materials, at length scales that range from several centimeters down to nanometers. This article illustrates our experiences with a few of these new developments, with some examples of how this traditional field continues to explode into new territory, enabling rapid acquisition of huge data sets on the one hand, while permitting exploration of chemical composition of targets with nanometer-scale spatial resolution on the other.

Methods

Targets

Samples for high spatial resolution, and for large-scale, rapid imaging, are taken from our studies on biological targets. Sample acquisition and tissue preparation are described elsewhere for snap-frozen mouse brain tissue (3) and rat heart (4). Healthy rat heart was cryosectioned at 7 µm from a frozen block that had been embedded in optimal cutting temperature medium (TissueTek OCT, Sakura). Normal mouse brain (C57BL/6) was similarly embedded and cryosectioned onto low-e reflective slides (MirrIR, Kevley Technologies). Near-field IR spectra and images have been used to assess yeast cell walls (*Saccharomyces cerivisiae*). Cells were grown in standard

agar medium overnight; a few drops of purified (MilliQ) water were placed onto the new growth, removed, and deposited onto either a gold-coated silicon wafer or a BaF_2 window. A purified water rinse was used to remove traces of medium.

High Spatial Resolution Imaging

Experiments for high spatial resolution imaging on a conventional Fourier transform infared (FT-IR) microscope with high numerical aperture (NA) optics and focal plane array (FPA) detection were performed on a commercial FT-IR microscope (Agilent Cary 620, with either 64x64 or 128x128 FPA, located in our lab at the University of Manitoba and the Advanced Light Source, Lawrence Berkeley National Laboratory, respectively). With 25x objectives (NA= 0.81) and a 128×128 FPA detector, image pixels have a nominal geometric spatial resolution of 3.3 µm. Optionally, additional magnification in front of the detector reduces this resolution value to a nominal 0.7 µm/pixel. Spectral acquisition and data processing were accomplished with the Resolutions-Pro FT-IR spectroscopy software.

Rapid Imaging of Large Tissue Sections

Experiments for rapid imaging of entire tissue sections were conducted with a prototype rapid scan instrument (Agilent Laser Direct Infrared [LDIR] Imaging Analyzer), equipped with a tunable quantum cascade laser (QCL), rapid scanning optics, and a single-point thermoelectrically cooled detector, and with conventional far-field IR microscopes, as described above.

sSNOM-Style Near-Field IR Nanospectroscopy

NFIR spectra and images have been acquired with the in-house designed or built synchrotron infrared nanospectroscopy (SINS) end station and a commercial scattering scanning near-field optical microscopy (sSNOM) instrument (Neaspec, GmbH), located at the Advanced Light Source, Lawrence Berkeley National Laboratory. Both instruments are illuminated by broadband synchrotron radiation.

Results

High Spatial Resolution Imaging

We have been testing the detail that can be achieved to distinguish physically distinct entities; in this case, that would be skeins of collagenous webbing that hold cardiomyocytes in heart muscle. For the normal magnification, far-field conventional microscope images (25x, 3.3 µm) example, healthy rat heart was cryosectioned at 7 µm and mounted on a BaF_2 window. The structure of the heart is designed for optimal torque as the cardiomyocytes contract and release, pumping blood through the vessels. The myocytes are arranged on a thin collagenous matrix (6,7).

The spectral signature of collagen Type I is well known, and is readily distinguished from normal muscle, given the differences in the amide bands, as well as the absence of lipid bilayer membranes in the collagen (Figure 1a). The cardiomyocytes were characterized by the symmetric CH_2 stretching band at 2852 cm^{-1}, and the collagen by the unique profile of the amide III region, with

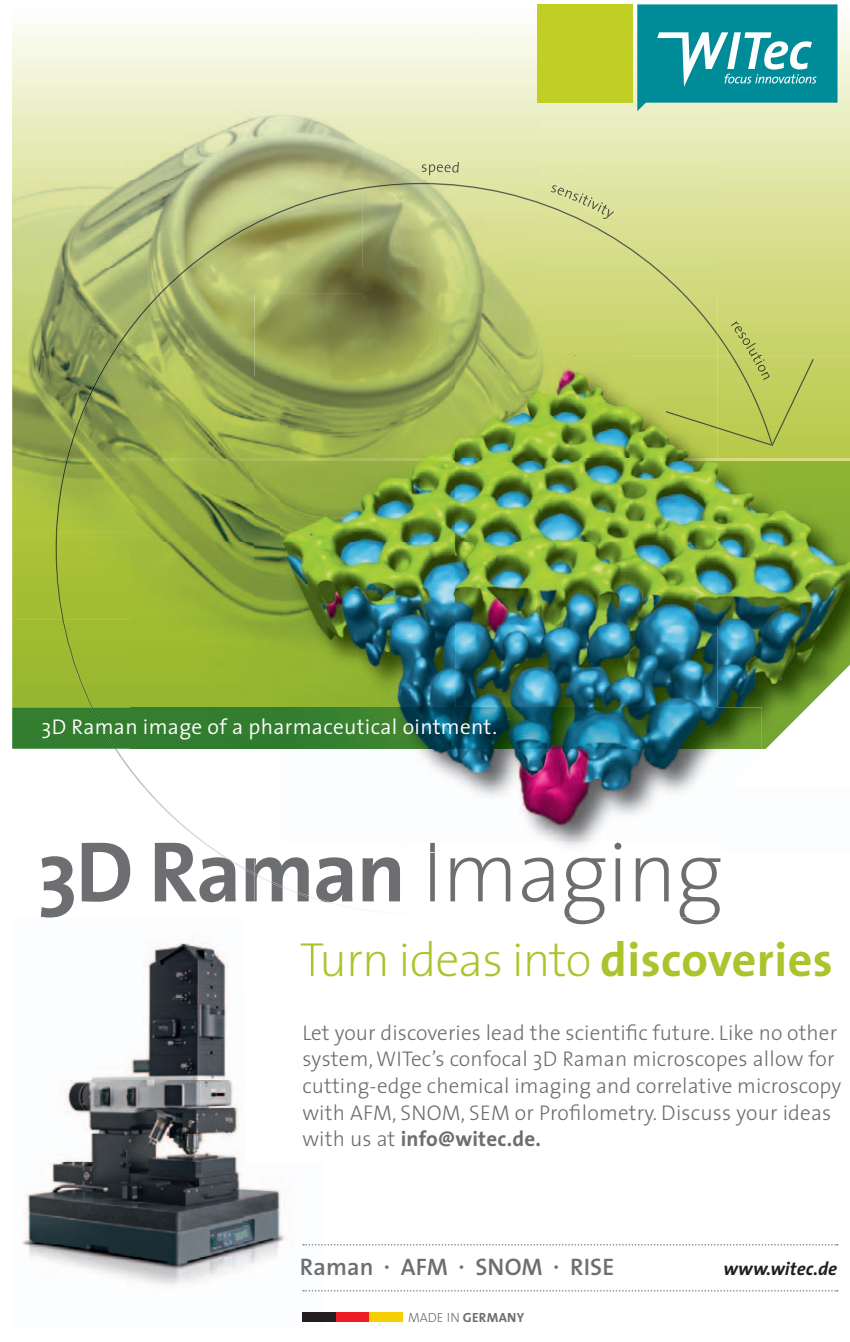

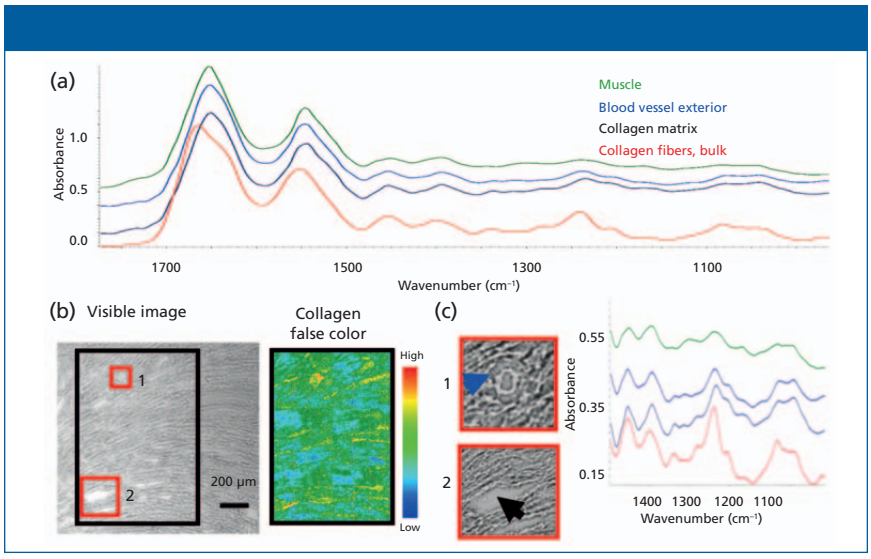

Figure 1: High spatial resolution imaging of cardiac section from rat heart reveals collagen anchoring blood vessels and binding myocytes to establish structure–function relationship.

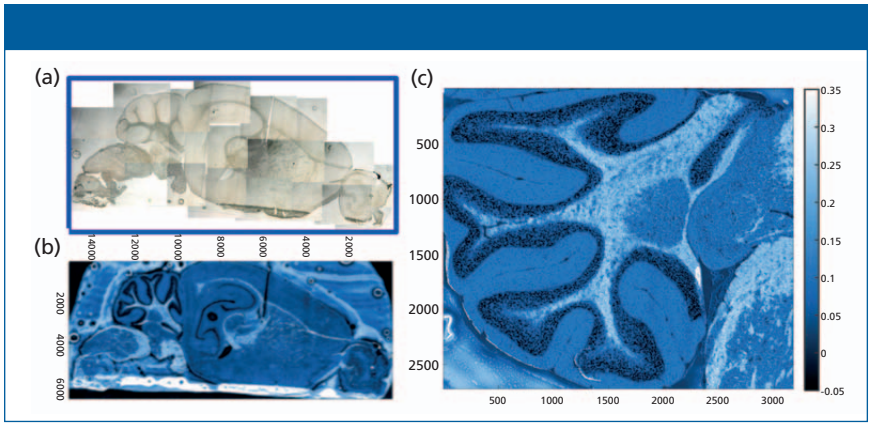

Figure 2: Single-wavelength contrast image of mouse brain section obtained with QCL tuned to lipid carbonyl at 1735 cm^{-1} against two baseline points. Pixel size: 5 µm; total pixels: 3.87M; total time: 10 min.

peaks at 1204, 1240, 1284, and 1337 cm^{-1}. The structure–function relationship is evident in the white light photomontage of the left ventricle (Figure 1b), where the arc of muscle cells indicates the direction of torsional action. The black box outlines the region imaged at 25x, normal magnification; the mosaic has been processed on the 1204 cm^{-1} collagen band. Although the heart muscle cells are thick and their infrared signature is easily discerned, it is much more difficult to detect the slender collagenous webbing that defines the heart structure. The white light image shows regions that might be collagen but the 25x objective with 3.3-µm pixels is required to isolate this faint tracery (red boxes 1 and 2, Figures 1c and 1d). Structural collagen holds blood vessels to the muscle cells (1, blue spectrum); the collagen matrix supports and defines the overall structure (2, black spectrum) (Figure 1d). Note: we found that the pixels with the 15x objective (5.5 µm) were too large, because collagen signal was lost within the adjacent cardiomyocytes, whereas use of the higher magnification optics (1.1 µm at 15x, or 0.7 µm at 25x) had a poorer signal-to-noise ratio, and again the collagen was hard to discern. These results illustrate some of the tradeoffs and choices required for such imaging, including considerations of key features in heterogeneous targets.

Rapid Imaging of Large Tissue Sections

A saggital section of mouse brain is several millimeters in length and width, a sample size that is common to numerous types of tissue section, whether heart, brain, or biopsy, and that size has presented significant challenges for infrared imaging. By binning multiple pixels, or imaging at preset large pixel sizes (20–50 µm), it is possible to cover the entire section, but depending on the setup, acquisition can still take several hours and the image pixilation becomes increasingly crude, so that critical information is lost. Two different solutions are shown here.

QCL, Single-Wavelength Contrast Imaging

A section mounted on a low-e glass slide (Figure 2a), imaged with the processed QCL image (Figure 2b), shows the gray matter and white matter contrast obtained from the intensity recorded at 1735 cm^{-1} (fatty acid ester carbonyl) relative to intensity at two baseline points. Pixel size is close to the diffraction limit for this wavelength, at 5 µm. The imaged area, 6.420 mm x 15.070 mm, consists of 3.87 x 106 pixels, and the elapsed time to acquire the image was only 10 min. In this simple contrast image, the darker pixels correspond to low lipid content, typical of cell bodies, and the white regions correspond to high lipid content, typical of white matter. The detail achievable is further highlighted in the expanded, higher resolution image of the cerebellum, with data collected as a sum of three scans, a nominal pixel dimension of 3 µm, and a total scan time of 7.3 min (Figure 2c). This approach, and other instruments based on QCL (7), allow for tissue imaging in effectively real time. Different implementations of this approach can result in scattering artifacts, but these can be addressed either with a focused beam, rapid scan instrument such as the one used here, or with post-processing of the specular scatter that arises from nonfocused QCL beams. Operation in transflectance mode introduces other scatter anomalies. However, whether in transmission or transflection, some scatter persists. Mathematical analyses and physical models to address these issues are being developed in tandem, but are beyond the scope of this article.

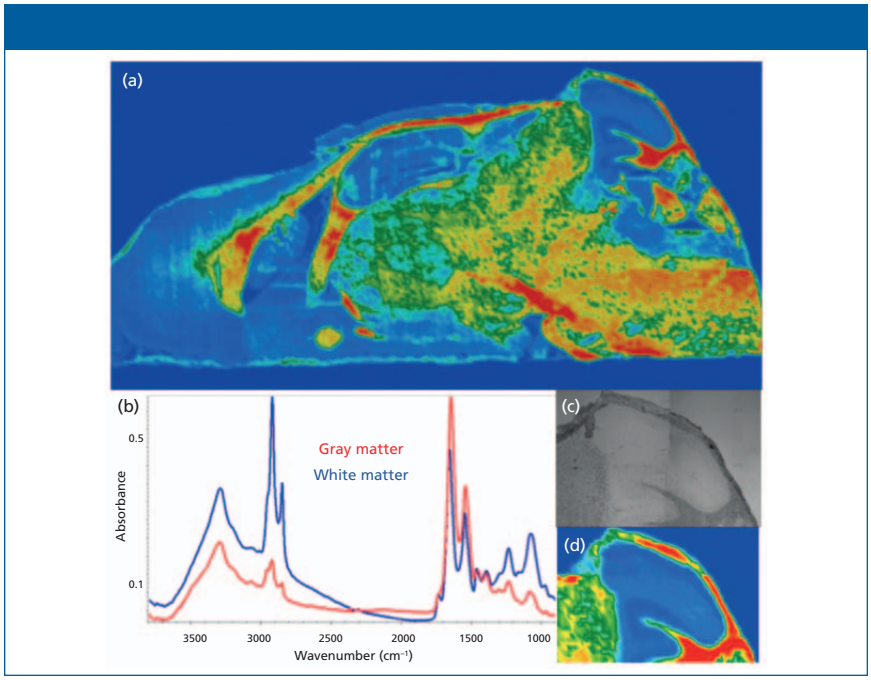

Figure 3: Conventional FT-IR mosaic image of mouse brain section mounted on low-e slide; processed on the integrated intensity of the symmetric CH stretch band at 2852 cm^{-1}.

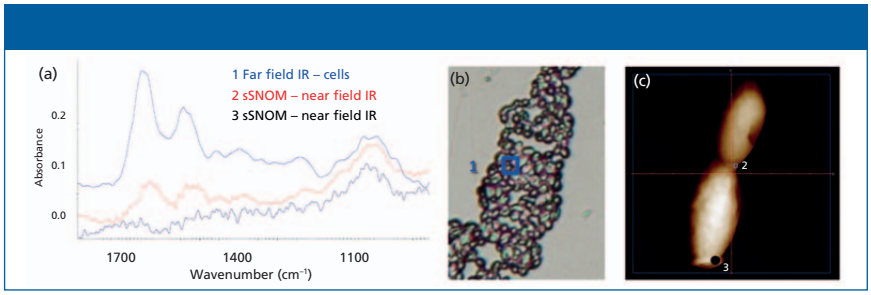

Figure 4: Far-field and near-field spectra from a cell of the common yeast *Saccharomyces cerevisiae*. Far-field IR spectra of cells were obtained in transmission for cells on a BaF_2 window and sSNOM-SINS spectra were acquired at the Advanced Light Source.

Far-Field, Full-Spectrum FT-IR Imaging with Conventional IR Microscope and Focal Plane Array

Similar images, in transflectance or transmission mode, can be obtained nearly as rapidly with a conventional FT-IR instrument and a large-area FPA detector.

The mosaic in Figure 3a was acquired at a nominal 5-µm pixel resolution, and consists of 130 tiles, or ~ 2.1 x 10^6 spectra. The false color image shows distribution of gray and white matter with the usual rainbow false-color processing from high (red) to low (blue), based on the lipid CH stretch band. By choosing a shorter wavelength, the sample image has been oversampled. Smaller pixels are still feasible, and fewer scans can still provide desired information. Spectra recorded at 8 cm^{-1} from this image are shown in Figure 3b, and a close-up of the cerebellum is shown in Figure 3c (visible image) and Figure 3d (processed on the integrated intensity of the same band). Although this image took about 50 min to acquire, the advantage here is that the entire spectrum (4000–900 cm^{-1}) is obtained at each pixel, allowing assessment of possible scattering and background issues, and the images are obtained in far less time than would be required if full spectra were sought with the QCL approach. The latter approach is most useful when speed of acquisition is critical and potential variations in the targets are well-characterized.

sSNOM-Style Near-Field IR Nanospectroscopy

Near-field IR techniques couple infrared light (synchrotron source or laser) to the

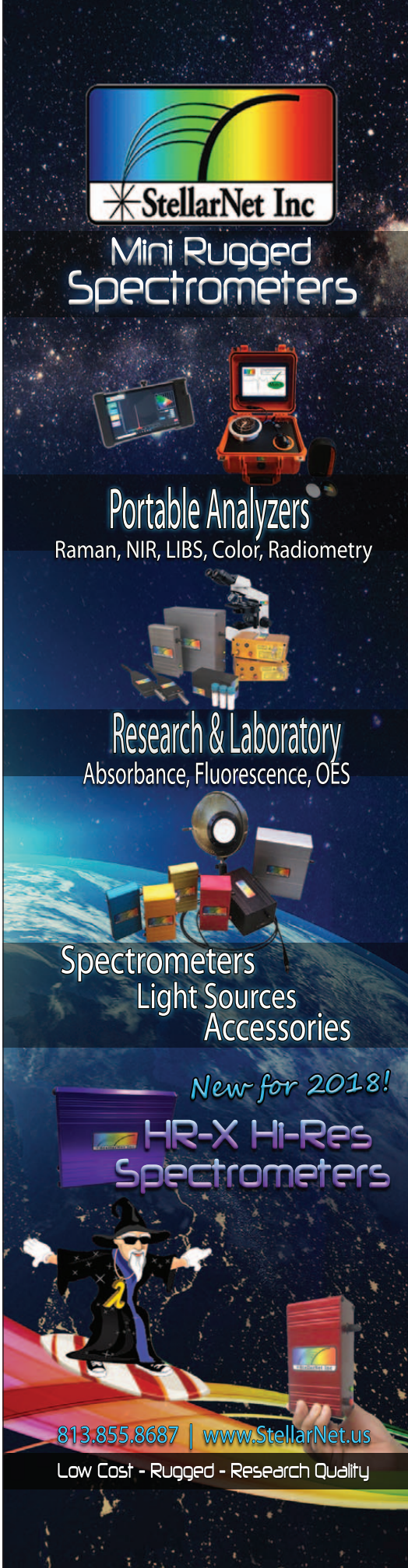

tip of an atomic force microscope for spatially resolved IR spectroscopy, and imaging well beyond the diffraction limit (8,9). Several implementations are now possible; we have used the sSNOM approach to achieve what appears to be the maximum resolution to date, with a probe voxel edge on the order of 20 nm (10).

A typical spectrum of the *S. cerevisiae* cell wall, extracted from the far-field FT-IR image, shows the expected protein amide bands and contributions from sugars, phosphates, and other cell content (Figure 4a, spectrum 1, blue), taken from the region inside the blue box in Figure 4b. In contrast, two near-field IR spectra acquired with the sSNOM SINS set up at Advanced Light Source are dominated by the polysaccharide wall composition (red and black spectra, Figure 4a) recorded at the budding tips (locations 2 and 3, Figure 4c). The ovoid shape of these cells made it difficult to obtain good spectra; however, these are the first such spectra obtained by sSNOM and improvements can be envisioned.

Conclusion

Rapid, detailed imaging of relatively large targets with far-field IR generates massive amounts of data. Near-field IR is still in its infancy, but is evolving quickly. Developments in both areas are creating excellent opportunities for new exploration at micrometer and nanometer length scales, ultimately for better macroscopic understanding.

Acknowledgments

Data collection and figure preparation were conducted by several members of my group: Negar Atefi, Tanvi Vakil, Zahra Abyat, Sarvesh Ramlochun, and Gorkem Bakir. Heart tissue was generously donated by Professor Ian Dixon, University of Manitoba; brain tissue was donated by Professor Benedict Albensi, University of Manitoba. Thanks to Dr. Hans Bechtel (ALS, LBNL, Berkeley) for assistance in the collection of near-field IR data and images; this research used resources of the Advanced Light Source, which is a DOE Office of Science User Facility under contract no. DE-AC02-05CH11231. Thanks are also extended to Dr. Chris Moon and Dr. Matthew Kole, Agilent Technologies. ZA and GB are supported by University of Manitoba GETS scholarships; NA and TV have received University of Manitoba Faculty of Science Undergraduate Research Awards. This work is funded by NSERC Canada and CIHR.

References

(1) P.R. Griffiths and J.A. de Haseth, *Fourier Transform Infrared Spectrometry* (John Wiley & Sons, New York, New York, 2006).
(2) M.J. Nasse, M.J. Walsh, E.C. Mattson, R. Reininger, A. Kajdacsy-Balla, V. Macias, R. Bhargava, and C.J. Hirschmugl, *Nat. Methods* **8**(5), 413–416 (2011).
(3) C.R. Findlay, R. Wiens, M. Rak, J. Sedlmair, C.J. Hirschmugl, J. Morrison, M. Kansiz, and K.M. Gough, *Analyst* **140,** 2493–2503 (2015).
(4) K.M. Gough, D. Zielinski, R. Wiens, M. Rak, and I.M.C. Dixon, *Analytical Biochem.* **316,** 232–242 (2003).
(5) H.C. Ott, T.S. Matthiesen, S.K. Goh, L.D. Black, S.M. Kren, T.I. Netoff, and D.A. Taylor, *Nat. Medicine* **14**(2), 213–221 (2008).
(6) K.T. Weber, *J. Am. Coll. Cardiol.* **13**(7), 1637–1652 (1989).
(7) C. Kuepper, A. Kallenbach-Thieltges, H. Juette, A. Tannapfel, F. Großerueschkamp, and K. Gerwert, *Sci. Rep.* **8,** 7717 (2018).
(8) H.A. Bechtel, E.A. Muller, R.L. Olmon, M.C. Martin, and M.B. Raschke, *PNAS* **111**(20), 7191–7196 (2014).
(9) F. Huth, A. Govyadinov, S. Amarie, W. Nuansing, F. Keilman, and R. Hillenbrand, *Nano Lett.* **12,** 3973–3978 (2012).
(10) R. Wiens,C. R. Findlay, S. G. Baldwin, L. Kreplak, J. M. Lee, S. P. Veres and K. M. Gough, *Farad. Discuss.* **187,** 555–573 (2016).

Kathleen Gough is a professor with the Department of Chemistry, and the Biomedical Engineering Program, at The University of Manitoba, Winnipeg, MB, Canada. Direct correspondence to: kathleen.gough@umanitoba.ca. **Tanya E.S. Dahms** is a professor at the Department of Chemistry and Biochemistry, University of Regina, Regina, SK, Canada. **Benedict C. Albensi** is a professor, and Manitoba Dementia Research Chair, at The University of Manitoba, Winnipeg, MB, Canada. **Ian M.C. Dixon** is a Principal Investigator Molecular Cardiology, Institute of Cardiovascular Sciences and Professor, Department of Physiology and Pathophysiology, at the University of Manitoba, Winnipeg. MB, Canada. **Negar Atefi, Tanvi Vakil, Zahra Abyat, Sarvesh K. Ramlochun,** and **Gorkem Bakir** are students with the Department of Chemistry, and the Biomedical Engineering Program, at The University of Manitoba, Winnipeg, MB, Canada.

The Spectroscopy Specialists

Pathlengths from 0.01mm to 100mm
Volumes from 0.6ul to 35ml
Far UV & NIR Quartz
Glass & Borosilicate

Starna Cells, Inc.
PO Box 1919 Atascadero, CA 93423
Starna
Phone: (800) 228-4482 USA or (805) 466-8855 outside USA
sales@starnacells.com www.starnacells.com

For more information on this topic, please visit our homepage at: www.spectroscopyonline.com

PRODUCTS & RESOURCES

Wavelength calibration sources

Ocean Optics' spectrometer wavelength calibration sources are designed in configurations that span the ultraviolet to the near infrared. According to the company, the wavelength calibration source series (-2 models) include mercury-argon (253–1700 nm), krypton (427–893 nm), neon (540–754 nm), argon (696–1704 nm), and xenon (986–1984 nm) gas-discharge emission sources.
Ocean Optics, Largo, FL;
https://oceanoptics.com/product/spectrometer-wavelength-calibration-sources/

Terahertz Raman high-throughput screening system

Ondax's TR-WPS automated well-plate measurement system is designed to combine high-throughput screening with low-frequency THz-Raman technology to identify and screen polymorphic compounds and co-crystals, or quantify degree of crystallinity in pharmaceuticals. According to the company, the system is compatible with standard well plates and custom substrates.
Ondax, Monrovia, CA;
www.ondax.com

CCD cameras

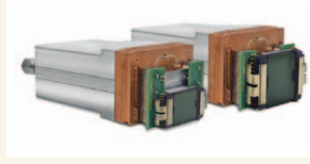

The PI-MTE3 charged-coupled device cameras from Princeton Instruments are designed for direct detection in vacuum ultraviolet (UV), extreme ultraviolet, and X-ray imaging applications from ~10 eV to 30 keV. According to the company, the cameras are suitable for applications such as X-ray microscopy, X-ray spectroscopy, X-ray phase contrast imaging, X-ray diffraction, deep-UV lithography, and semiconductor metrology.
Princeton Instruments,
Trenton, NJ;
www.princetoninstruments.com

Protein characterization system

The AQS³ Pro protein characterization system from RedShift BioAnalytics, Inc. is designed with integrated bioanalytics software for spectroscopic analysis in the development, formulation, and manufacture of biotherapeutics. According to the company, the system is based on microfluidic modulation spectroscopy and allows users to see change in the secondary structure of proteins over the concentration range of 0.1–200 mg/mL.
RedShift BioAnalytics, Burlington, MA; www.redshiftbio.com

X-ray diffraction system

Rigaku's sixth-generation MiniFlex X-ray diffraction system is designed as a multipurpose analytical instrument that can determine phase identification and quantification, percent crystallinity, crystallite size and strain, lattice parameter refinement, Rietveld refinement, and molecular structure. According to the company, the system includes a HyPix-400 MF 2D hybrid pixel array detector, an available 600-W X-ray source, and an eight-position automatic sample changer. **Rigaku Corporation,** Tokyo, Japan;
www.rigaku.com/en/products/xrd/miniflex

Automated electric fusion fluxer

The Katanax X-300 fluxer from Spex SamplePrep is designed to produce fused beads for X-ray fluorescence or inductively coupled plasma solutions for analysis. According to the company, the benefits of electric fluxers versus gas fluxers include safety, temperature control, low power consumption, and simple installation.
Spex SamplePrep,
Metuchen, NJ;
www.spexsampleprep.com/x300-fluxer

Modular fluorescence systems

Wasatch Photonics' fluorescence spectrometers are designed with a high NA input and transmissive VPH gratings to reduce acquisition time. According to the company, the spectrometers are available for 400–800 nm or 400–1800 nm wavelength ranges in fiber-coupled or free-space models.
Wasatch Photonics,
Durham, NC;
www.wasatchphotonics.com

XRF kit

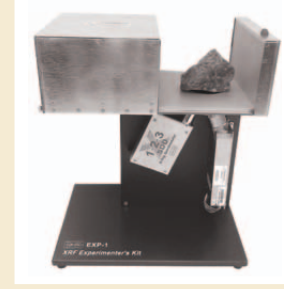

Amptek's XRF kit is designed to help users quickly begin doing elemental analysis via X-ray fluorescence. According to the company, the kit includes the company's X-123 complete spectrometer with a FAST SSD or SSD detector, a Mini-X USB Controlled X-ray tube, XRF-FP QA software, a sample enclosure, and test sample.
Amptek, Inc.,
Bedford, MA;
www.amptek.com

Optical isolators

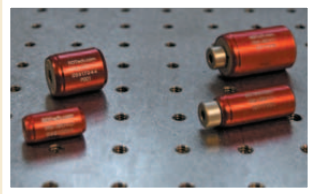

EOT's compact Tornos Series optical isolators are designed to provide high transmission in the forward direction while strongly attenuating light traveling in the reverse direction. According to the company, the isolators allow for isolation and transmission at a specific wavelength within the spectral bandwidth of the isolator.
Electro-Optics Technology, Inc.,
Traverse City, MI;
www.eotech.com

Raman analyzer

The RamanRXN2 Multichannel analyzer from Kaiser is designed to provide high-resolution, research-grade Raman spectra on a portable platform for process development monitoring and control. According to the company, a single analyzer can collect Raman data from four channels, addressable by fiber-optic probes capable of direct in situ liquid or solid measurements in applications ranging from from raw materials identification to process control in a manufacturing environment.
Kaiser Optical Systems, Inc.,
Ann Arbor, MI;
www.kosi.com

Fluorescence instruments & accessories

PerkinElmer's FL 6500 and FL 8500 fluorescent spectrometers are designed for sample testing. According to the company, the instruments use interchangeable, plug-and-play accessories, intuitive software, and support services.
PerkinElmer, Inc.
Waltham, MA
www.perkinelmer.com

Portable hydraulic press

The Pixie portable hydraulic press from PIKE Technologies is designed for making high-quality KBr pellets. According to the company, users can make pellets by turning a knob, and the press's small footprint makes it suitable for limited bench-space environments and glove boxes, and for ease of storage. The press reportedly is capable of applying a force of as high as 2.5 tons.
PIKE Technologies,
Madison, WI;
www.piketech.com

Raman polymer analysis application note

An application note from Renishaw describes how Raman imaging provides the power and flexibility to investigate all polymer types to provide chemical information and high-resolution 2D and 3D chemical images. According to the company, applications range from investigation of polymer crystallinity, and understanding coating layers, to identification of microplastic contamination in the environment.
Renishaw, Hoffman Estates, IL; www.renishaw.com/polymers

Polymer fluorescent references

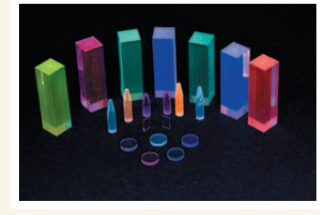

Starna's second-generation polymer fluorescent references are designed for wavelength calibration and the monitoring of instrument performance in fluorescent applications. According to the company, the new references are based on new proprietary dyes and provide increased stability and resistance to photobleaching, allowing for their use as relative photometric intensity references.
Starna Cells, Inc., Atascadero, CA;
www.starnacells.com

Portable Raman analyzer

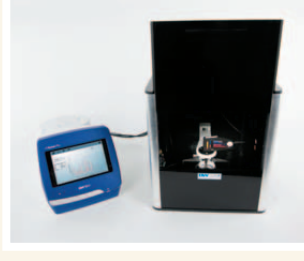

B&W Tek's Carbon Raman analyzer is designed as aportable system with 532-nm laser excitation and a fiber-optic sampling probe. According to the company, the analyzer is suitable for materials in powdered forms, and eliminates the need for sample preparation or for a microscope.
B&W Tek,
Newark, DE;
www.bwtek.com/products/portable-carbon-raman-analyzer

Inverted confocal 3D Raman imaging microscope

WITec's alpha300 Ri confocal Raman imaging microscope is designed with an inverted beam path. According to the company, the ability to view and investigate samples from below is an advantage when working with aqueous solutions and oversized samples, and the microscope is suitable for studies in life sciences, biomedicine, pharmaceuticals, and geosciences.
WITec GmbH, Ulm, Germany;
www.witec.de

Electron backscatter diffraction camera

The Velocity EBSD camera from EDAX is designed for highspeed electron backscatter diffraction mapping. According to the company, the camera combines indexing speeds greater than 3000 indexed points per second with indexing success rates of 99% or better, and image resolution that provides orientation precision values of less than 0.1°.

EDAX, Inc.,
Mahwah, NJ;
www.edax.com

Diffraction database

The PDF-4+ 2019 database from ICDD is designed for phase identification and quantitative analysis. According to the company, the database includes 412,083 entries with digital patterns for use in total pattern analysis; 312,395 entries with I/Ic values for quantitative analysis by reference intensity ratio; and 311,225 entries with access to atomic coordinates sets for quantitative analysis by the Rietveld method.

International Centre for Diffraction Data,
Newtown Square, PA; www.icdd.com

X-ray diffraction system

Malvern Panalytical's Empyrean X-ray diffraction and scattering system is designed to perform a variety of complementary X-ray experiments without manual intervention. According to the company, the system can automatically optimize resolution and intensity.

Malvern Panalytical,
Malvern, UK;
www.malvernpanalytical.com/en

Direct mercury analyzer

Milestone's DMA-80 direct mercury analyzer is designed to provide results that are comparable to traditional techniques in as little as 5 min per sample. According to the company, the analyzer has the ability to analyze virtually any matrix.

Milestone, Inc.,
Shelton, CT;
milestonesci.com/direct-mercury-analyzer/

Extending the reach of portable Raman

Today's Raman spectroscopy demands higher signal, less noise, and faster measurements than ever before. We deliver.

- Spectrometers & systems, 405–1064 nm
- Configurable, from coupling to cooling
- Demos available!

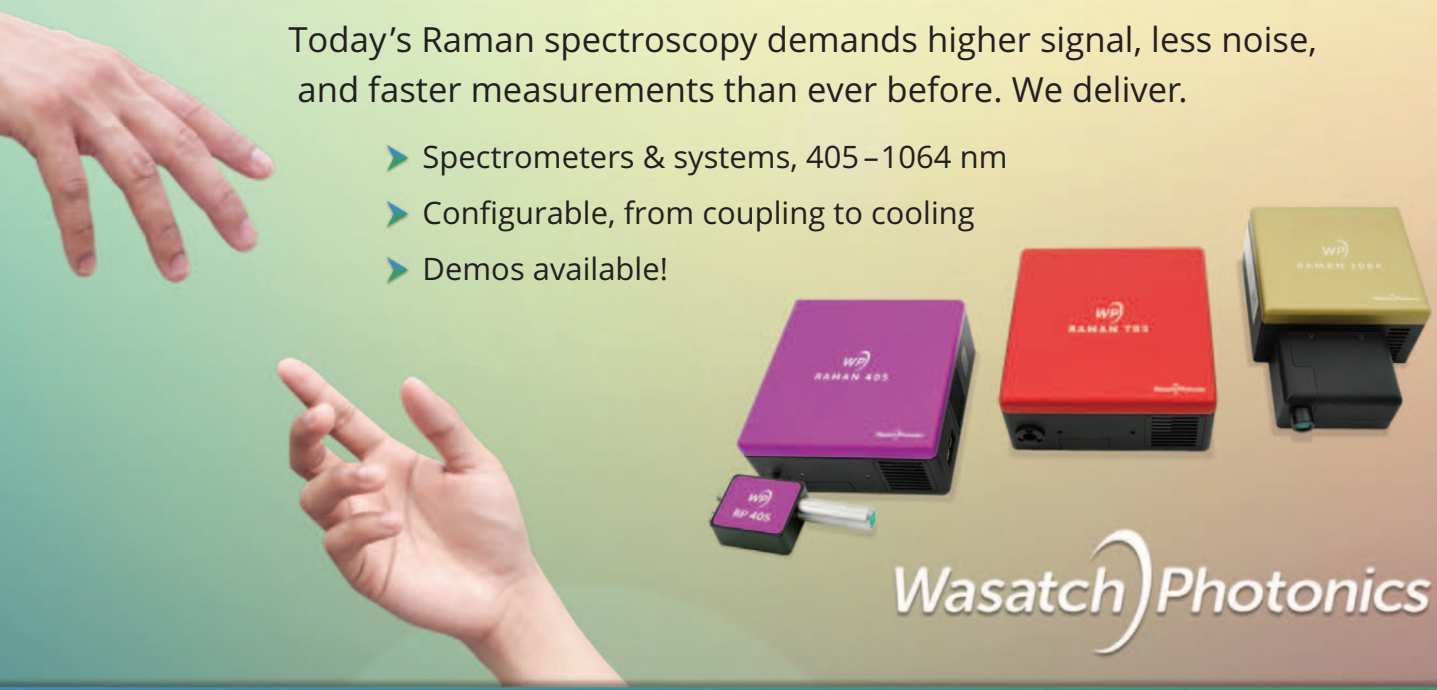

RAMAN | UV-VIS | FLUORESCENCE | NIR

+1 919-544-7785 • info@wasatchphotonics.com • wasatchphotonics.com

Precision NMR Sample Tubes & Sampling Accessories

Quality and value you can rely on!

Standard and Special Applications

New Era Enterprises, Inc.
Ph: 1-800-821-4667 Fax: 1-856-697-8727
cs@newera-spectro.com www.newera-spectro.com

Low Frequency Raman Filters

Stokes and anti-Stokes modes at 5 cm^{-1} and up

Available wavelengths 400-2500 nm

405, 442, 458, 473, 488, 491, 514, 532, 552, 561, 568, 588, 594, 632, 660, 785, 830, 980, 1064, 1550

OptiGRATE
HIGH EFFICIENCY FOR HIGH POWER

Ad Index

ADVERTISER	PG#
ACD/Labs	21
Amptek Inc.	3
art photonics GmbH	25
Avantes BV	50
B&W Tek, Inc.	15
CEM Corporation	CV Tip
Eastern Analytical Symposium	6
Edinburgh Instruments	4
Electro-Optics Technology	4
Hamamatsu Corporation	17
Inorganic Ventures IV Labs	11
Milestone Inc.	9, 45
Moxtek, Inc.	48
MRS Spring	23

ADVERTISER	PG#
New Era Enterprises Inc.	42
Ocean Optics, Inc.	51, CV2
Ondax, Inc.	31
OptiGrate Corporation	42
PerkinElmer Corporation	46–47, CV4
PIKE Technologies	7, 52
Princeton Instruments	5
Renishaw, Inc.	10
Rigaku GMG	13, 49
Spex SamplePrep	19
Starna Cells, Inc.	6, 38
StellarNet, Inc.	37
Stranaska LLC	53
Thermo Fisher Scientific	CV3
Wasatch Photonics, Inc.	41
WITec GmbH	35, 54

Supplement to
Spectroscopy®
Solutions for Materials Analysis
September 2018
www.spectroscopyonline.com

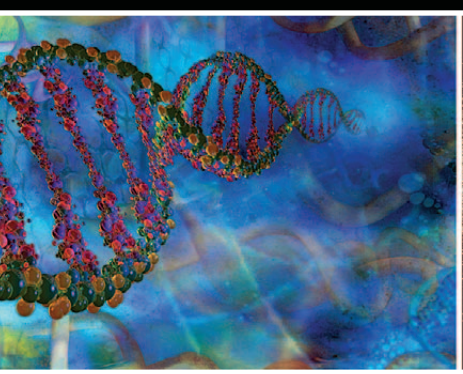

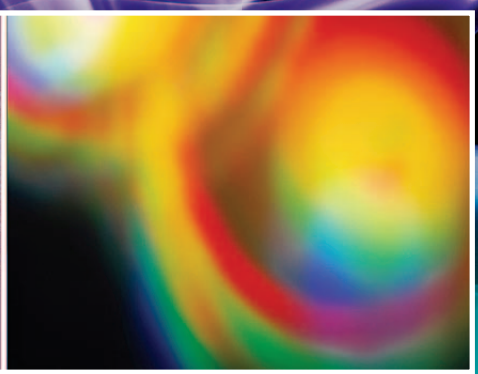

THE APPLICATION NOTEBOOK

UBM

THE APPLICATION NOTEBOOK

Atomic Spectroscopy

45 **Microwave Sample Prep for Heavy Metals Determination in Accordance with USP <232>/<233>**

Milestone, Inc.

46 **The Benefits of SP-ICP-MS to Assess the Fate of Nanoparticles During the Coagulation of Drinking Water**

A. Donovan and H. Shi, Missouri University of Science, and C. Stephan, PerkinElmer, Inc.

48 **Miniature 70 kV, 12W X-ray Source**

Sterling Cornaby, PhD, Moxtek

49 **Operando Measurement of Li Ion Battery Positive Electrode in Charge/Discharge Process by X-ray Diffraction**

Rigaku Corporation

Molecular Spectroscopy

50 **Biomedical Fluorescence Applications**

Avantes, Inc.

51 **Volume Fraction Determination of Ethanol in a Splash-Blended Fuel Mixture**

Derek Guenther, Ocean Optics

52 **Automated ATR for High-Throughput Laboratories**

Jenni L. Briggs, and Lorenz Sykora†, *PIKE Technologies, †IRUBIS GmbH*

53 **Advances in Cobalt-Nickel-Nitrate Reference Solutions for Qualification of Analytical Absorption Spectrophotometers**

Jerry Messman, Melissa Hartwell, Doug Martinez, and Jeff Crawford, Stranaska Scientific LLC

54 **Inverted Confocal Raman Imaging for Life Sciences**

Wolfram Ibach, Andrea Richter, Karin Hollricher, WITec GmbH

MILESTONE
HELPING CHEMISTS

Microwave Sample Prep for Heavy Metals Determination in Accordance with USP <232>/<233>

Milestone, Inc.

Single reaction chamber (SRC) microwave digestion offers significant benefits over traditional microwave digestion for pharmaceutical samples: higher sample throughput, reduced labor and consumables costs, simplified workflow and superior digestion quality.

Summary

New USP chapters <232> and <233> for the measurement of inorganic contaminants in pharmaceutical samples have been implemented. While samples can be dissolved in aqueous or organic solvents, the large majority will require digestion, and closed-vessel microwave digestion is stipulated by USP. Single reaction chamber (SRC) microwave digestion is a new type of closed vessel digestion that was developed by Milestone and offers many advantages over closed vessel digestion—particularly for pharmaceutical sample types.

Two sample types, St. John's wort and fish oil, typical of finished product pharmaceuticals, were digested using an SRC digestion system and analyzed for the four toxic USP elements using collision-cell ICP-MS. Since all samples are digested together in a single chamber, duplicates and spike recoveries were performed to confirm the retention of volatile elements and the absence of cross contamination.

St. John's Wort
Parts per million (µg/g)

Step	Arsenic	Cadmium	Lead	Mercury
Sample result	0.184	0.109	0.24	ND
Duplicate result	0.195	0.115	0.19	ND
Detection limit	0.008	0.003	0.03	0.1

Fish Oil Gelcaps
Parts per million (µg/g)

Step	Arsenic	Cadmium	Lead	Mercury
Sample result	0.007	ND	0.018	0.035
Duplicate result	0.006	ND	0.022	0.024
Detection limit	0.002	0.007	0.007	0.008

Quality Control Summary (Fish Oil Gelcaps)
Parts per million (µg/g)

Step	Arsenic	Cadmium	Lead	Mercury
Spike conc	15.3	5.09	10.2	15.3
Spike result	15.6	5.15	9.96	14.2

The data above show excellent DLs and recovery—even for the volatile element mercury. There is no loss of volatiles or cross-contamination with the UltraWAVE.

Instrumentation

The Milestone UltraWAVE can digest up to 15 samples simultaneously, at up to 300 °C and 199-bar pressure. Its high temperature and pressure capability enables the complete digestion of virtually every sample type. Samples are weighed into vials and placed in the chamber: and any combination of sample types can be digested together, greatly simplifying the sample prep workflow. Raw materials, excipients, API, and final product can all be digested together in the same run. And the UltraWAVE uses disposable glass vials, eliminating vessel assembly/disassembly and vessel cleaning, which significantly reduces labor and consumables costs. Most pharmaceutical sample types have high organic content, including oils and fats, which are difficult to digest and generate CO_2 which increases pressure in the reaction vessel. The high pressure capability of the UltraWAVE enables it to digest entire fish oil gelcaps—not possible with traditional closed vessel microwave.

The UltraWAVE can digest samples in as little as 3 mL acid which minimizes reagent blank levels – important since ICP-MS will be used predominantly for USP <232>/<233>. The SRC chamber is prepressurized with N_2 prior to the start of the run. This prevents sample boiling, eliminating cross-contamination and loss of volatiles.

Conclusion

Milestone's UltraWAVE SRC microwave digestion system offers multiple benefits for sample preparation and subsequent analysis.

Due to its higher sample capacity, use of disposable vials, and faster cool down time, the UltraWAVE's sample throughput is 2x–3x higher than closed vessel digestion. Its lower consumables costs, simple operation, and superior digestion quality also make the Milestone UltraWAVE the perfect choice for pharmaceutical sample prep.

Milestone, Inc.
25 Controls Drive, Shelton, CT 06484
tel. (866) 995-5100, fax (203) 925-4241
Website: www.milestonesci.com

PerkinElmer®
For the Better

The Benefits of SP-ICP-MS to Assess the Fate of Nanoparticles During the Coagulation of Drinking Water

A. Donovan*, H. Shi*, and C. Stephan†, *Missouri University of Science & Technology and †PerkinElmer, Inc.

The continued application of engineered nanoparticles (ENPs) raises concerns about their introduction into natural water bodies via wastewater discharge, incorrect disposal, and leaching from outdoor applications. If discharged into surface water, the fate of ENPs in drinking water treatment processes needs to be evaluated. Coagulation is one of the primary treatments used to remove particles from drinking water; thus, understanding the fate of ENPs during typical coagulation processes is required to accurately predict human exposure. Single particle ICP-MS (SP-ICP-MS) is an important advancement in environmental monitoring of ENPs that has the capability to quickly evaluate size, concentration, and dissolved metal concentration simultaneously with minimal sample preparation.

With many ENPs utilized in consumer products, this work focused on five common varieties: Ag, Au, TiO_2, ZnO, and CeO_2. The fate of these particles through coagulation processes in two surface water types was evaluated using SP-ICP-MS. Zone 4 coagulation process (aka *sweep floc*) was used for these experiments. Sweep floc occurs when coagulant is added past the point of solubility, creating insoluble flocs that aggregate. Other particles in the water are attracted to the coagulant flocs and are removed during sedimentation.

Experimental

Citrate-stabilized Ag (40, 70, and 100 nm dia) and Au (50, 80, and 100 nm dia) NPs in 2 mM sodium citrate were purchased from nanoComposix, Inc. (San Diego, CA). Uncoated TiO_2 (100 nm), CeO_2 (30–50 nm), and ZnO NPs (80–200 nm) were purchased from US Research Nanomaterials, Inc. (Houston, TX), and prepared in DI water. Dissolved Ag, Au, Ti, Ce, and Zn standards in DI water were used to calibrate the instrument.

To simulate coagulation processes, the most commonly used coagulants, including aluminum sulfate, ferric chloride and ferric sulfate, were purchased from Thermo Fisher Scientific, Inc. (Pittsburgh, PA). River water and lake water samples were collected from the Missouri River, and Schuman Lake in Rolla, MO, respectively. Samples were taken from just below the surface, two feet from the bank. Precleaned polypropylene bottles were used to collect samples, and stored in the refrigerator until use.

Instrumentation and SP-ICP-MS Methods

A NexION® ICP-MS with Syngistix™ Nano Software Module (PerkinElmer Inc., Shelton, CT) was used for sample analysis and data processing, using ^{47}Ti, ^{107}Ag, ^{197}Au, ^{67}Zn, ^{140}Ce for quantitation.

Coagulation Treatments

A six-gang stirrer with 2-L square beakers was used for the coagulation treatments (Phipps and Bird). Following the addition of water, 70 nm Au (5 µg/L), 80 nm Ag (2 µg/L), 100 nm TiO_2 (6 µg/L), 30–50 nm CeO_2 (5 µg/L), and 80–200 nm ZnO (6 µg/L) nanoparticles were added to the beakers and dispersed by stirring. Predetermined amounts of coagulants were added to the beakers and stirred at decreasing speeds to simulate flocculation and sedimentation. Samples were taken immediately after dispersion and after sedimentation to evaluate the change in particle size, concentration, and dissolved ion concentration.

Results

Data demonstrating the change in size distribution histograms of Ag ENPs in river water and lake water after Zone 4 coagulation with three different coagulants are provided in Figure 1. "NO TREATMENT" samples were water matrix with ENPs added and were stirred and underwent sedimentation but did not have coagulant added. "BEFORE TREATMENT" samples were collected from each beaker immediately after the ENPs were dispersed. No obvious shift in size was observed after each treatment. However, the decrease in frequency indicates that the ENPs were removed to some degree after each treatment.

ENP Fate During Coagulation

The change in ENP particle concentration after various coagulation treatments was studied in river and lake water. Particle-size-distribution histograms were generated for each treatment and each particle type. Combined distributions for each particle type are shown in Figures 2 and 3 for river water and lake water, respectively. Particle concentrations decreased after each treatment for all ENPs. The water matrix impacted size distributions, likely due to differences in dissolved organic carbon (DOC). CeO_2 ENPs showed greater stability in high DOC lake water compared to lower DOC river water, as indicated by a mean particle size closer to that of the primary particles in the standard. ZnO is known to be highly soluble in water, thus particle size will vary based on water chemistry. In this case, particles aggregated more in lake water compared to river water. In control samples ("NO TREATMENT"), the particle size and concentration was similar before and after treatment for most particles, showing stability between the time of ENP addition and final sampling. ZnO ENPs exhibited dissolution over time when no treatment was applied due to its known solubility in water.

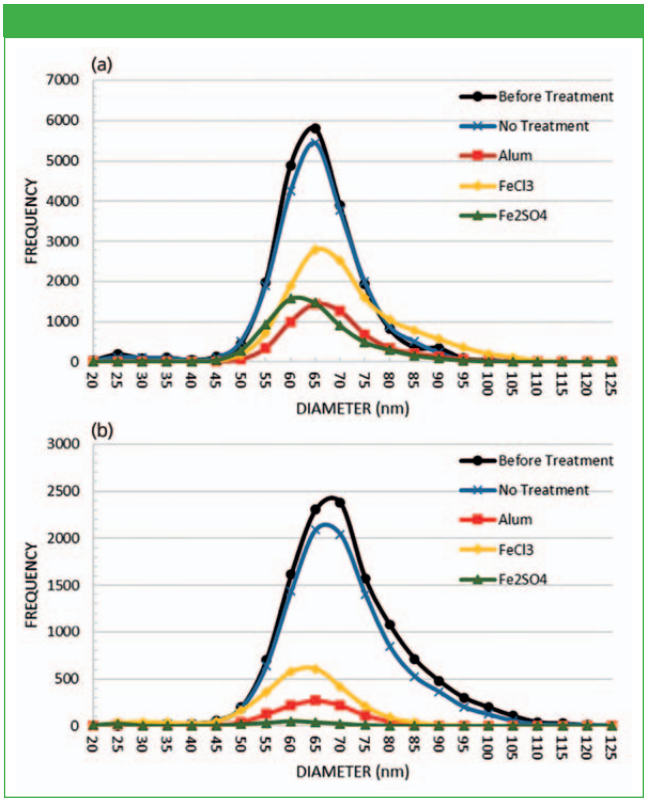

Figure 1: Change in size distribution histograms for Ag ENPs during various coagulation treatments in (a) river water and (b) lake water.

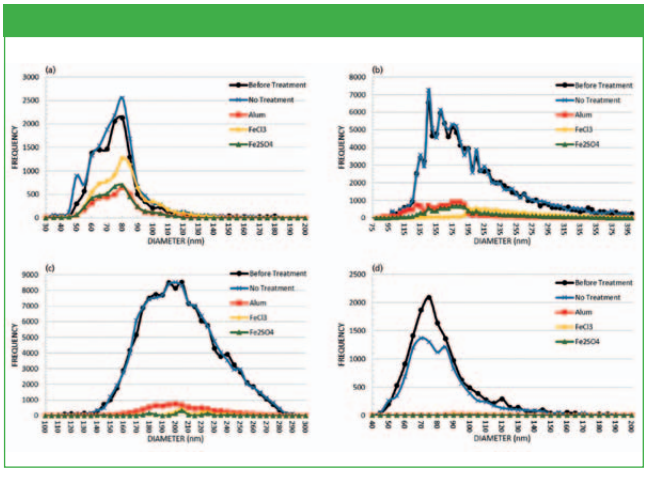

Figure 2: Size distribution histograms for (a) Au, (b) TiO_2, (c) CeO_2, and (d) ZnO ENPs after Zone 4 coagulation treatments using various coagulants in river water.

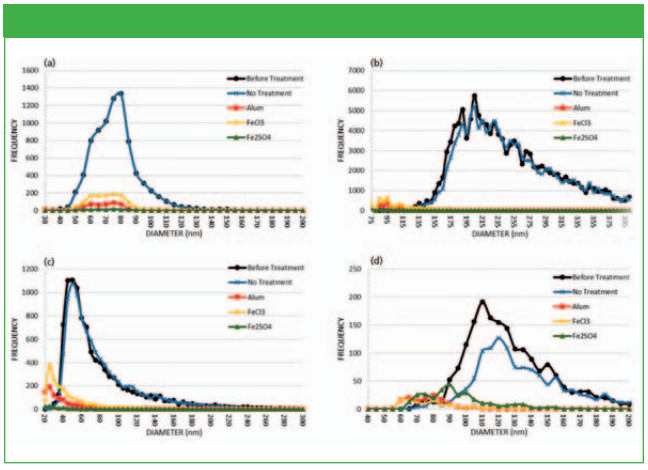

Figure 3: Size distribution histograms for (a) Au, (b) TiO_2, (c) CeO_2, and (d) ZnO ENPs after Zone 4 coagulation treatments using various coagulants in lake water.

Though it won't be discussed in detail here, total ENP removal was improved when polymer was added as a coagulant aid. This result was expected due to the cross-linking nature of the polymer during floc formation. Compared to citrate-stabilized ENPs, uncoated TiO_2, CeO_2, and ZnO ENPs were more efficiently removed across all treatments in river water, likely due to the lower average surface charge resulting in more charge neutralization and aggregation.

Conclusions

Monitoring ENPs during drinking water treatment is important as their use in consumer and commercial products continues to rise. This work has demonstrated SP-ICP-MS, using PerkinElmer's NexION ICP-MS with Syngistix Nano Software Module, to be a good technique to monitor the particle size and concentration of ENPs in surface waters. This study has also shown that the efficacy of coagulation to remove ENPs from surface waters is an important parameter to consider for risk assessments.

Download the full application note at
www.perkinelmer.com/nexion2000

PerkinElmer, Inc.
940 Winter Street, Waltham, MA 02451
tel. (800) 762-4000 or (+1) 203-925-4602
Website: www.perkinelmer.com

Miniature 70 kV, 12W X-ray Source

Sterling Cornaby, PhD, Moxtek

Recently, the compact* MAGPRO's *maximum voltage was increased from 60 kV to 70 kV while maintaining the same size profile. This article highlights the advantages of 70 kV excitation of cadmium, an element of interest for the Restriction of Hazardous Substances Directive (RoHS), at parts per million (ppm) levels.

The MAGPRO 12 W miniature source is small and low power, which is an advantage for a number of applications. Our 12 W source has several anode materials available: a tungsten anode for either XRF or in X-ray imaging, as well as Rh, Ag, Cr, Cu, and Mo. The entire X-ray source (tube plus high voltage power supply) weights about 700 g (25.0 oz) and can be controlled by your choice of USB, digital, or analog control, and has an interlock connection for X-ray safety (Figure 1). The increase of high voltage from 60 kV to 70 kV for the MAGPRO was primarily motivated for use in handheld imaging applications. This increase in voltage also shows important benefits for spectroscopy applications as well. This article highlights the advantages of the 70 kV excitation for low levels of cadmium.

Experimental Conditions and Results for XRF Detection of Cadmium

Cadmium detection is of interest because it is a toxic metal that needs to be detected for RoHS/WEEE compliance. Detection of cadmium at low concentrations is particularly difficult because cadmium's 23.2 keV K_α emission line is much higher than that of other toxic elements of interest. An X-ray source with a higher voltage helps to increase the X-ray signal from cadmium. For this experiment, we used a typical XRF setup where the sample is placed at 45° to the tube and detector. The X-ray spot on the sample was 4×6 mm, achieved with a collimator and a tube-to-sample distance of 25 mm. A 200 µm molybdenum foil was placed between the tube and sample to suppress the Compton background scattering roughly between 20 to 30 keV; thereby suppressing the background under the cadmium K_α peak. Figure 2 shows four spectra taken from a polyvinyl chloride sample with 10 ppm of Cd, with the tube set at 40, 50, 60, and 70 kV. A 42 mm^2 SDD collected the data with a 15 mm sample-to-detector distance over 180 s live time, with the input count rate ranging from 20 to 100 kcps. It is evident that increasing the voltage also increases the cadmium signal. In this set-up, 10 ppm of cadmium is detectable in a reasonable 3–5 min time frame.

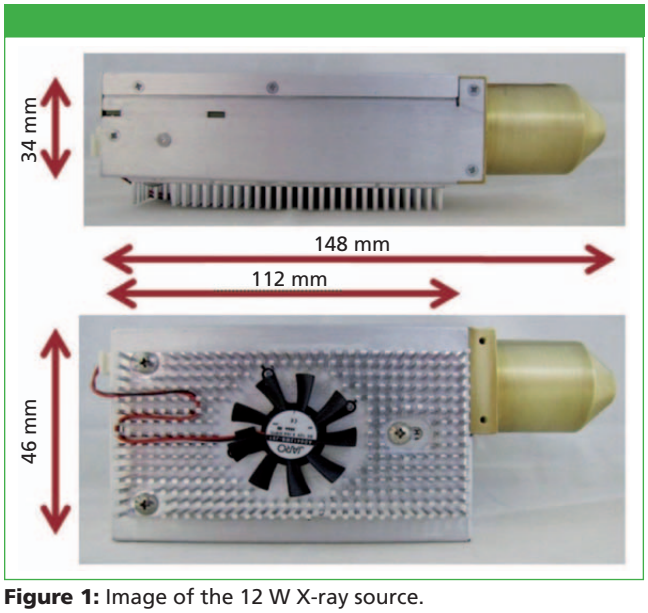

Figure 1: Image of the 12 W X-ray source.

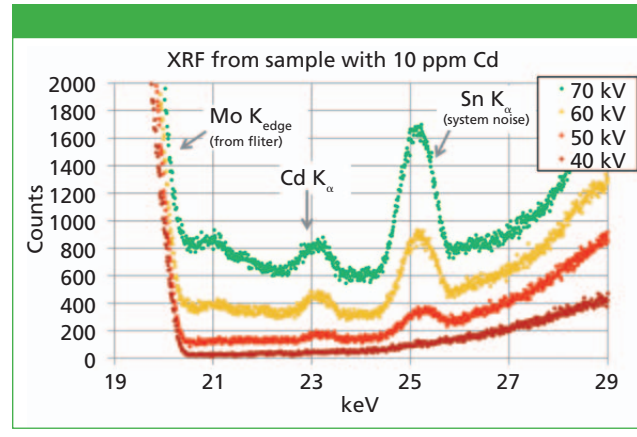

Figure 2: The cadmium line at about 23.2 keV gets larger as the voltage on the tube is increased. This is an advantage for cadmium detection in XRF systems looking for toxic metal at low concentrations.

Conclusion

The MAGPRO source is meant for use in small benchtop systems where small size is valued. It has increased its high voltage range from 60 kV to 70 kV, which is an advantage in detecting higher atomic number elements such as the hazardous substance cadmium.

Moxtek
452 West 1260 North, Orem, UT 84057
tel. (800) 758-3110
email: info@moxtek.com
Website: www.moxtek.com

Rigaku
Leading With Innovation

Operando Measurement of Li Ion Battery Positive Electrode in Charge/Discharge Process by X-ray Diffraction

Rigaku Corporation

This application note demonstrates the measurement by X-ray diffraction (XRD) of positive electrode material from lithium ion batteries during the charge/discharge process.

Lithium ion secondary batteries are widely used in small portable devices such as mobile phones. Research and development of lithium ion batteries for use in automobiles and larger machines is an active field. To develop lithium ion secondary batteries with high capacity, high stability and long life, it is essential to evaluate the stability of the positive electrode material during the charge/discharge process. Operando X-ray diffraction measurements using an attachment that reproduces the charge/discharge environment and a 2D detector that can perform high-speed measurements enables detailed observation of crystal phase changes while a battery is in use, making it suitable for studying battery performance and life.

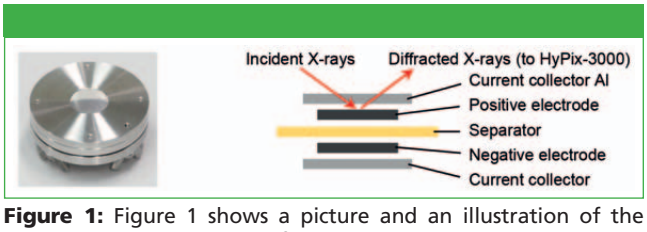

Figure 1: Figure 1 shows a picture and an illustration of the cross-sectional structure of a battery cell attachment. The positive electrode material was $LiMn_{1.5}Ni_{0.5}O_4$. Measurement using an exposure time of 15 s was repeated while charging/discharging the electrode at a charge and discharge rate 1C = 132 mAh/g. Changes to the X-ray diffraction profile over time were investigated.

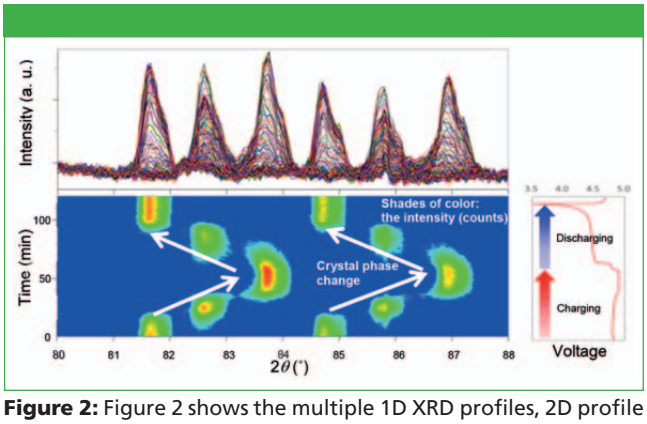

Figure 2: Figure 2 shows the multiple 1D XRD profiles, 2D profile maps and voltage graphs. Two steps of a two-phase coexistence reaction occurred with charging and discharging. After charging and discharging, the electrode material returned to the same crystal phase as before the measurement started.

Figure 3: Rigaku SmartLab automated multipurpose X-ray diffractometer (XRD) with Guidance software.

Experimental Conditions

X-ray diffraction measurements of the positive electrode material during high-speed charging and discharging were carried out with a battery cell attachment and a HyPix-3000 2D detector on a Rigaku SmartLab X-ray diffractometer.

Conclusion

The Rigaku SmartLab Automated multipurpose X-ray diffractometer with HyPix-3000Hybrid pixel array multi-dimensional detector can perform high-speed Operando measurements of crystal phase changes of lithium ion batteries to evaluate battery performance and life.

Rigaku Corporation
9009 New Trails Drive, The Woodlands, TX 77381
tel. (281) 362-2300, fax (281) 364-3628
Website: www.rigaku.com

AVANTES
enlightening spectroscopy

Biomedical Fluorescence Applications

Avantes, Inc.

Many biomedical research applications exploit the natural fluorescence response of amino acids, the essential building blocks of all proteins. These protein fluorescence responses have been used for everything from pharmaceutical manufacturing to biowarfare defense.

Intro to Proteins and Amino Acids

Proteins, the complex organic compounds made of chains of amino acids, are the most abundant organic molecule in all living things on Earth. They act as catalysts, regulate physiological processes, and they defend the body against disease.

Three common amino acids, tryptophan, tyrosine, and albumin, responsible for the majority of inherent fluorescence, have a common structure of hydrogen-based rings. These ring structures, called *aromatic hydroxyl groups,* absorb UV radiation and emit a weak fluorescent signal at varying wavelengths.

Fluorescence in Action: Cancer Fighting Weapons

Spectroscopy has proven to be invaluable in the fight against cancers. In lung cancer detection, for example, use of autofluorescence bronchoscopy employs a narrow probe inserted through the patient's mouth into the upper bronchial tree.

Autofluorescence has been shown to be far more sensitive than white light bronchoscopy in the detection of carcinomas or dysplastic lesions, but it also has a high rate of false positives. Researchers at the Department of Respiratory Diseases in Rotterdam, the Netherlands (1), are investigating the use of absorbance/reflection optical spectroscopy to improve specificity without losing sensitivity.

Using a specially designed probe to fit the 2.8 mm bronchoscope channel, the mucosa tissue was irradiated with a tungsten/halogen broadband light source and a blue laser calibrated to 407 nm. The resulting reflectance and fluorescence emissions were collected via a multichannel Avantes spectrometer installation equivalent to two AvaSpec-ULS2048CL-EVOs in parallel.

The emission peak for autofluorescence of healthy tissue was 500 nm. Areas that display an abnormal fluorescence profile can be rapidly targeted for additional spectral measurements which can be acquired in <1 s. Diseased tissue displayed drastically lower emission intensity at shorter wavelengths compared to healthy tissues. The combined autofluorescence imaging and optical reflectance spectroscopy significantly improved the positive predictive value compared with autofluorescence alone without sacrificing sensitivity.

Experimental Design

The Avantes Engineering team reproduced a series of experiments (2) conducted with samples of tryptophan, tyrosine, and bovine serum albumin to demonstrate our protein detection capabilities. The team used conventional absorbance techniques with a continuous wave (CW) illumination source (AvaLight-DHc) and an AvaSpec-ULS3648-USB2 spectrometer configured for UV (190–400 nm). Absorption measurements, recorded between 190–320 nm, correlated changes in concentration to changes in absorption. Fluorescence was not measured during this experiment.

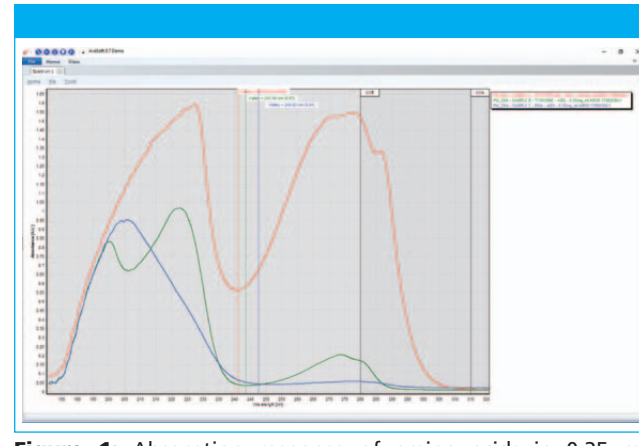

Figure 1: Absorption response of amino acids in 0.25 mg concentration solution.

The team running this experiment prepared three different concentrations for each of the three sample analytes: 1 mg/mL, 0.5 mg/mL, and 0.25 mg/mL, and took broadband absorption spectra profiles for each.

Results

The absorption profiles of the amino acids correlated directly with the amino acid concentration in solution. As fluorescence is a function of absorbance and quantum yield, the fluorescence can be estimated and would be expected to also correlate with concentration.

References

(1) M.P.L. Bard et al., "Improving the specificity of fluorescence bronchoscopy for the analysis of neoplastic lesions of the bronchial tree by combination with optical spectroscopy," *Lung Cancer* **47**(1), 41–47 (2005).

(2) P. Held, "Quantitation of peptides and amino acids with a Synergy™ HT using UV fluorescence." B.-T. Instruments, Winooski, VT (2003).

Avantes USA
500 S. Arthur Ave., Unit 500, Louisville, CO 80027
tel. +1 (303)-410-8668
Website: www.avantes.com

Volume Fraction Determination of Ethanol in a Splash-Blended Fuel Mixture

Derek Guenther, Ocean Optics

There are two primary methods of blending ethanol into gasoline: match blending and splash blending. Match blending aims to achieve some specified boiling point for the mixture and is primarily done with aromatics, resulting in a dirtier emission profile versus splash blending. Splash blending is the primary method used in the United States and is based on percent volume, specifically aiming to achieve 10% ethanol by volume in the final mix (Environmental and Energy Study Institute, 2014). In this study, we look at the Ocean Optics MZ5 MIR Spectrometer's ability to determine volume fraction of ethanol in a splash-blended fuel mixture using MIR spectroscopy.

Experimental Setup

In the world of fuel octane ratings, the 0-mark is set by *n*-heptane while the 100-mark is set by *i*-octane, also known as 2,2,4-trimethylpentane (Compound Interest, 2016). Focusing on the latter, mixtures were made using *i*-octane (99.8%) and 200-proof ethanol from Millipore Sigma. The following volume fractions were prepared:

Table I.

φ*i*-octane	φEtOH
0.00	1.00
0.50	0.50
0.75	0.25
0.80	0.20
0.90	0.10
1.00	0.00

Sample fluids were placed onto the crystal and measured. The MZ5's Mirror software saved the processed absorbance spectra.

The MZ5-MIR-ATR spectrometer offers excellent spectral response from 910-1810 cm^{-1} and is a robust measurement system for petroleum products and general process organics. Its simplified fixed-crystal design eliminates fiber connections and the movement/vibrational issues that come with their use.

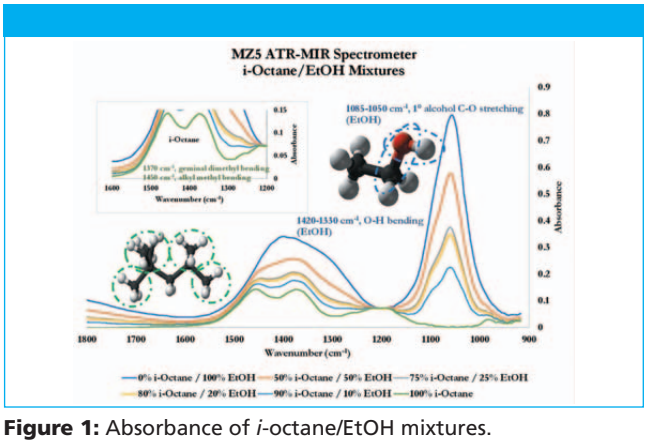

Figure 1: Absorbance of *i*-octane/EtOH mixtures.

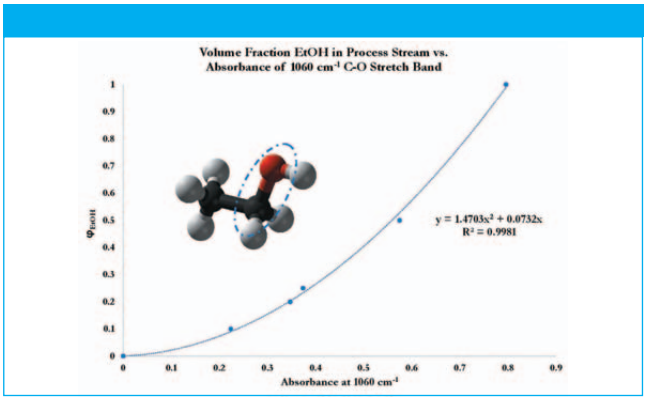

Figure 2: Absorbance trend of C-O stretch band.

Results

Figure 1 shows the resulting spectra for the ethanol mixtures described in Table I, along with some explanations for the activities and how they relate to the organic structures.

Traditional Absorbance Model

The ethanol activity is clearly the dominant influencer to these spectra, which is highly useful in determining its concentration both in the lab and on the process line. While there are two regions of large alcohol activity, the C-O stretch band is both the largest and the most independent of the *i*-octane profile. Plotting the volume fraction versus this absorbance trend provides a strong correlation (Figure 2).

Conclusion

The MZ5 is more than a spectrometer—it is a window into the molecular structures and concentrations of the chemicals in your process stream. In addition, Ocean Optics can provide users with algorithm development and machine learning tools that derive additional insight from the spectral data the MZ5 collects. Tools can be developed and refined to handle complex fuel mixtures and account for interference issues to provide readings that are robust and trusted.

Ocean Optics
8060 Bryan Dairy Rd., Largo, FL 33777
tel. (727) 733-2447
Website: www.OceanOptics.com

PIKE TECHNOLOGIES
Spectroscopic Creativity

Automated ATR for High-Throughput Laboratories

Jenni L. Briggs*, and Lorenz Sykora†, *PIKE Technologies, †IRUBIS GmbH

Using an automated ATR accessory, mid-infrared spectra were collected on 24 individual ATR crystals. Spectra were compared to a spectrum collected using a single bounce diamond ATR crystal. Advantages of implementing automated measurements and benefits of automation in laboratory environments are discussed.

ATR is one of the most popular mid-infrared sampling techniques because minimal to no sample preparation is required due to the short effective pathlength. Until now, automating ATR methods to improve workflow in high-throughput laboratories has been elusive because of the typical need to clean and dry the ATR sampling surface in between each measurement. By taking advantage of unique Si wafers functionalized with multiple microprisms optimized to perform as ATR elements, ATR automation is available as a commercial macroscale accessory. This application note explores automated ATR measurements in the evaluation of an organic solvent.

Experimental conditions

The model sample was propanol-2. Using the AutoATR Accessory by PIKE Technologies, a microtiter style platform for automated ATR measurements, 24 unique sample measurements were made on individual ATR crystals from IRUBIS GmbH. The accessory is suitable for measuring liquids, gels, pastes, and casted films. The AutoATR stage is controlled and data collection is initialized by PIKE AutoPRO7 software. Spectra collected with the AutoATR were compared with a single reflection diamond ATR. Spectral resolution was 8 cm^{-1} and 16 scans were co-added. Before the automated sample measurements an individual background was acquired for each well.

Results

The AutoATR uses 24 unique Si ATR elements, which have a thickness of 500 microns. Due to the thin profile of the crystal, the absorbance from Si phonon bands is minimal relative to thicker traditional Si ATR crystals. This allows the entire mid-IR spectral range to be accessed from 5000–400 cm^{-1}. Si has an extremely inert sampling surface and is suitable for use with substances having a pH between 1–12. The efficiency of the accessory's base optics and Si ATR element coupled with several microprisms results in high energy throughput and reproducibility.

Figure 1 shows 24 individual spectra of propanol-2 and a comparison spectrum collected using the PIKE MIRacle single reflection diamond ATR. Spectra collected with the AutoATR were exceptionally reproducible. In the fingerprint region the variance was less than 0.007 AU (no baseline correction implemented). Relative to a single reflection diamond ATR, the absorbance bands were almost two times stronger when collected with the AutoATR. Thus, this accessory will result in higher signal-to-noise ratio and greater sensitivity.

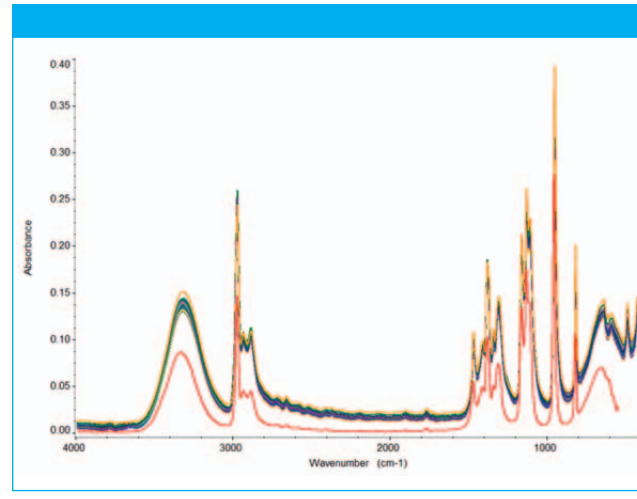

Figure 1: 24 individual ATR spectra of propanol-2 collected using the AutoATR and a spectrum collected with the MIRacle single reflection diamond ATR (red) for comparison.

The AutoATR high-throughput accessory is ideal for comprehensive larger studies. Fields of biology, medicine, pharmaceutics, and food could benefit from an automated ATR. Additionally, there are ongoing efforts to transfer infrared spectroscopy from academic research into clinics. An automated ATR device fulfills this requirement and enables larger studies, while increasing lab efficiency and minimizing workforce requirements.

Conclusion

New innovations in ATR elements in conjunction with an automated optical platform has made automated ATR measurements possible. Using the AutoATR, spectral results are more sensitive than a typical single reflection ATR.

PIKE Technologies, Inc.
6125 Cottonwood Drive, Madison, WI 53719
tel. (608) 274-2721
Website: www.piketech.com

STRANASKA
INNOVATION IN ANALYTICAL METROLOGY

Advances in Cobalt-Nickel-Nitrate Reference Solutions for Qualification of Analytical Absorption Spectrophotometers

Jerry Messman, Melissa Hartwell, Doug Martinez, and Jeff Crawford, Stranaska Scientific LLC

The major drawback of a potassium dichromate (PDC) reference solution intended for checking the accuracy of the photometric scale of an analytical absorption spectrophotometer is its lack of broad wavelength coverage. Two different PDC reference solutions are required to cover both the ultraviolet and visible regions of the spectrum. This application note describes a cobalt-nickel-nitrate (CNN) reference solution that is permanently sealed in a fused-silica cuvette. In contrast to PDC reference solutions, a single CNN solution/cuvette filter can be used in both the ultraviolet and visible spectral regions of the spectrum.

Standard mixtures of cobalt, nickel, and nitrate ions in aqueous perchloric acid were originally formulated in 1972 by Burke and Deardorff. The reference solutions were sealed in glass ampoules and issued in consumable form as SRM 931. Despite its exceptional popularity in today's modern analytical testing laboratories, SRM 931 is limited in its overall use because of the demanding requirements for careful handling, contamination control, and precise and skillful manipulations to ensure accurate transfer of a CNN reference solution into a separate cuvette for analysis. This restrictive feature of SRM 931 could be overcome by simply sealing the CNN solutions in fused-silica cuvettes.

CNN Solution/Cuvette Filters

The CRM 200 reference standard, first introduced in 1994, features many of the same positive attributes of SRM 931, with the added advantage that the reference solutions are permanently sealed in fused-silica cuvettes as shown in Figure 1. Further improvements in CNN solution/cuvette filters resulted with the introduction of the CA2M 706 reference standard in 2014 as part of the company's commemorative MAVRO series, and later again in 2016 with rebranding of the CRM 200 reference standard. The Stranaska® CRM 200 and CA2M 706 reference standards are distinguishable by their differing scopes of calibration and levels of scientific metrological rigor integrated into the calibration models that underpin their respective certifications. A comparison of the different CNN liquid absorbance standards is presented in Table I.

Table I: Comparison of cobalt-nickel-nitrate reference solutions

	NIST SRM 931 Series	Stranaska® CRM 200	Stranaska® CA2M 706
Solution container	Glass ampoule	Fused-silica cuvette	Fused-silica cuvette
Certification model	Batch	Individual	Individual
Measurement methodology	High-accuracy calibration	Routine calibration	Advanced calibration
Recertification status	Consumable	Recertification	Recertification

Figure 1: CNN solution/cuvette filters from Stranaska Scientific.

Recertification

The major advantage of Stranaska® CRM 200 and CA2M 706 reference standards is that each solution/cuvette filter is individually certified so that it can be used repeatedly over time. However, it is recommended that the reference standards be returned periodically to Stranaska Scientific for science-based recertification in order to clean the cuvettes, and to update the certified reference values and uncertainties.

Conclusions

The Stranaska® CRM 200 and CA2M 706 reference standards, which are derived from the SRM 931 series, are proven alternatives to PDC solutions for performance evaluation and qualification of analytical absorption spectrophotometers in FDA-regulated laboratories. The CNN solution/cuvette filters are more convenient to use by metrologists, engineers, and calibration technicians that do not have meaningful experience in common analytical laboratory practices.

Stranaska Scientific LLC
4025 Automation Way, Building A, Fort Collins, Colorado 80525
tel. (970) 282-3840
Website: www.stranaska.com

Inverted Confocal Raman Imaging for Life Sciences

David Steinmetz, Wolfram Ibach, Andrea Richter, and Karin Hollricher, WITec GmbH

Confocal Raman imaging is well suited to investigating biological specimens. The inverted beam path of the Raman microscope alpha300 Ri is especially useful for imaging samples in liquids such as cells and tissues.

Optical microscopy using fluorescence labeling cannot employ more than a handful of labels in one experiment, restricting the number of molecules that can be analyzed. This limitation does not apply to the label-free Raman imaging as the Raman effect is caused by the inelastic scattering of monochromatic light by the sample's molecules. Each type of molecule in a sample can be identified unambiguously by its individual Raman spectrum. By combining Raman spectroscopy with confocal microscopy the spatial distribution of the compounds within a sample can be visualized (1). It has been successfully applied for the investigation of organic materials (2–6).

3D Confocal Raman Imaging of Plant Pulp

The confocal microscope setup enables the generation of 3D Raman images by stacking 2D images of a series of focal planes. Here, a pressed piece of banana pulp mixed with water was investigated with an alpha300 R*i* inverted confocal Raman microscope (WITec). The scan range was $300 \times 200 \times 90\ \mu m^3$ with $450 \times 300 \times 45$ pixels. At each pixel a complete Raman spectrum was acquired. The integration time was 34 ms/spectrum. The 3D reconstruction of the Raman image stack (Figure 1) shows starch grains (green) and cell wall components (red).

Correlative Fluorescence and Raman Imaging of Eukaryotic Cells

Though strong fluorescence is the "natural enemy" of the weaker Raman signal, correlative fluorescence–Raman imaging using one microscope is possible by choosing a suitable laser wavelength, to avoid signal overlap. Kidney cells (Vero ATCC CCL-81) were grown in a petri dish. Nuclei were stained with DAPI. Cells were imaged in aqueous solution under the alpha300 R*i* microscope with a laser wavelength of 532 nm. An image of $50 \times 40\ \mu m^2$ with 150×120 pixels was generated. The acquisition time was 0.2 s/spectrum. The resulting correlative Raman–fluorescence image shows the nuclei (blue) imaged by fluorescence microscopy and the nucleoli (green) and endoplasmic reticula (red) imaged by confocal Raman microscopy based on their Raman spectra (Figure 2). The fluorescent dye does not interfere with the Raman measurement.

References

(1) J. Toporski, T. Dieing and O. Hollricher (eds.), *Confocal Raman Microscopy,* **66,** Springer International Publishing (2018).
(2) S. Richter, J. Müssig and N. Gierlinger, *Planta* **233,** 763–772 (2011).
(3) B. Prats-Mateu et al., *Biotechnology Journal* **12,** 1600037 (2017).
(4) P. Heraud, et al., *Scientific reports* **7,** 8949–8954 (2017).
(5) Kallepitis et al., *Nat. Commun.* **8,** 14843–18851, (2017).
(6) H.K. Yosef et al., *Anal. Chem.* **89,** 6893–6899 (2017).

WITec GmbH
Lise-Meitner-Str. 6, 89081 Ulm, Germany
tel. +49 (0)731 140 700, fax +49 (0)731 140 70 200
Website: www.witec.de

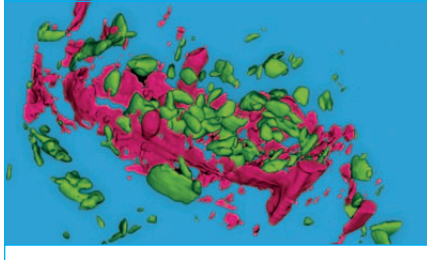

Figure 1: Raman image of banana pulp with starch grain marked in green, cell wall material in red.

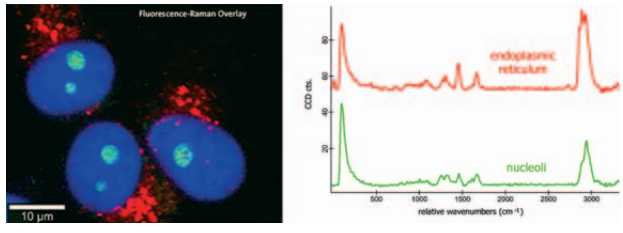

Figure 2: Correlative Raman–fluorescence image showing DAPI-stained nuclei (blue). Nucleoli (green) and endoplasmic reticula (red) were identified by their Raman spectra.

thermo scientific

analyze develop solve improve innovate test discover study

Nicolet™ iS50 FTIR Spectrometer

validate assure document review

What did you do today?

Whether you're discovering new materials, solving analytical problems or assuring product quality, your spectrometer needs to deliver the definitive answers you're looking for — fast! Thermo Fisher Scientific goes beyond your expectations with a full line of FTIR, NIR and Raman spectroscopy systems, to help you move from sample to answer . . . faster than ever before.

The Thermo Scientific™ Nicolet™ iS50 FTIR Spectrometer is your all-in-one materials analysis workstation. With simple one-touch operation and fully-integrated diamond ATR, the Nicolet iS50 gives your lab the productivity you need today and the capabilities you need tomorrow.

Discover. Solve. Assure. **thermofisher.com/solve-is50**

ThermoFisher SCIENTIFIC

For Research Use Only. Not for use in diagnostic procedures. © 2017 Thermo Fisher Scientific Inc. All rights reserved. All trademarks are the property of Thermo Fisher Scientific and its subsidiaries unless otherwise specified.
AD52971 0017

FLUORESCENCE
THAT OUTSHINES EXPECTATIONS

FL 6500™ and FL 8500™ Fluorescence Spectrometers

Copyright © 2018 PerkinElmer, Inc. 400382_01 All rights reserved. PerkinElmer® is a registered trademark of PerkinElmer, Inc. All other trademarks are the property of their respective owners.

We know that high performance and reliability are top priorities for labs. We've developed a complete fluorescence solution that enables confident, precise sample testing. Designed to work as fluidly as you do, our spectroscopy instruments use interchangeable, plug-and-play accessories, intuitive software that mirrors your laboratory workflow, and support and services that validate your equipment and ensure you meet standard compliance regulations. Tackle any application challenge that comes your way.

For more information, visit www.perkinelmer.com.

PerkinElmer®
For the Better